1 **Optical control of ERK and AKT signaling promotes axon regeneration and functional**

2 **recovery of PNS and CNS in *Drosophila***

3 Qin Wang[1,2], Huaxun Fan[3], Feng Li[1,2], Savanna S. Skeeters[3], Vishnu Krishnamurthy[3], Yuanquan

4 Song[1,2,]*, Kai Zhang[3,4,5,6,]*

5 [1]Raymond G. Perelman Center for Cellular and Molecular Therapeutics, The Children's Hospital

6 of Philadelphia, Philadelphia, PA 19104, USA

7 [2]Department of Pathology and Laboratory Medicine, University of Pennsylvania, Philadelphia,

8 PA 19104, USA

9 [3]Department of Biochemistry, [4]Neuroscience Program, [5]Center for Biophysics and Quantitative

10 Biology, [6]Beckman Institute for Advanced Science and Technology, University of Illinois at

11 Urbana-Champaign, Urbana, IL 61801, USA

12 *Correspondence and requests for materials should be addressed to Y.S. (email:

13 songy2@email.chop.edu) or to K.Z. (email: kaizkaiz@illinois.edu).

14

15 **Abstract**

16 Neuroregeneration is a dynamic process synergizing the functional outcomes of multiple

17 signaling circuits. Channelrhodopsin-based optogenetics shows feasibility of stimulating neural

18 repair but does not pin down specific signaling cascades. Here, we utilized optogenetic systems,

19 optoRaf and optoAKT, to delineate the contribution of the ERK and AKT signaling pathways to

20 neuroregeneration in live *Drosophila* larvae. We showed that optoRaf or optoAKT activation not

21 only enhanced axon regeneration in both regeneration competent and incompetent sensory

22 neurons in the peripheral nervous system, but also allowed temporal tuning and proper guidance

23 of axon regrowth. Furthermore, optoRaf and optoAKT differ in their signaling kinetics during

24 regeneration, showing a gated versus graded response, respectively. Importantly in the central

25 nervous system, their activation promotes axon regrowth and functional recovery of the

26 thermonociceptive behavior. We conclude that non-neuronal optogenetics target damaged

27 neurons and signaling subcircuits, providing a novel strategy in the intervention of neural

28 damage with improved precision.

29

30 **Introduction**

31 Inadequate neuroregeneration remains a major roadblock towards functional recovery after

32 nervous system damage such as stroke, spinal cord injury (SCI), and multiple sclerosis.

33 Extracellular factors from oligodendrocyte, astroglial, and fibroblastic sources restrict axon

34 regrowth (Liu et al. 2006; Yiu and He 2006; Liu et al. 2011; Lu et al. 2014; Schwab and

35 Strittmatter 2014) but eliminating these molecules only allows limited sprouting (Sun and He

36 2010), suggesting a down-regulation of the intrinsic regenerative program in injured neurons

37 (Sun and He 2010; He and Jin 2016). The neurotrophic signaling pathway, which regulates

38 neurogenesis during embryonic development, represents an important intrinsic regenerative

39 machinery (Ramer et al. 2000). For instance, elimination of the PTEN phosphatase, an

40 endogenous brake for neurotrophic signaling, yields axonal regeneration (Park et al. 2008).

41 An important feature of the neurotrophin signaling pathway is that the functional

42 outcome depends on signaling kinetics (Marshall 1995) and subcellular localization (Watson et

43 al. 2001). Indeed, neural regeneration from damaged neurons is synergistically regulated by

44 multiple signaling circuits in space and time. However, pharmacological and genetic approaches

45 do not provide sufficient spatial and temporal resolutions in the modulation of signaling

46 outcomes in terminally differentiated neurons *in vivo*. Thus, the functional link between

2

47   signaling kinetics and functional recovery of damaged neurons remains unclear. The emerging

48   non-neuronal optogenetic technology uses light to control protein-protein interaction and enables

49   light-mediated signaling modulation in live cells and multicellular organisms (Zhang and Cui

50   2015; Khamo et al. 2017; Johnson and Toettcher 2018; Leopold et al. 2018; Dagliyan and Hahn

51   2019; Goglia and Toettcher 2019). By engineering signaling components with photoactivatable

52   proteins, one can use light to control a number of cellular processes, such as gene transcription

53   (Motta-Mena et al. 2014; Wang et al. 2017), phase transition (Shin et al. 2017; Dine et al. 2018),

54   cell motility (Wu et al. 2009) and differentiation (Khamo et al. 2019), ion flow across

55   membranes (Kyung et al. 2015; Ma et al. 2018), and metabolism (Zhao et al. 2018; Zhao et al.

56   2019), to name a few. We have previously developed optogenetic systems named optoRaf

57   (Zhang et al. 2014; Krishnamurthy et al. 2016) and optoAKT (Ong et al. 2016), which allow for

58   precise control of the Raf/MEK/ERK and AKT signaling pathways, respectively. We

59   demonstrated that timed activation of optoRaf enables functional delineation of ERK activity in

60   mesodermal cell fate determination during *Xenopus laevis* embryonic development

61   (Krishnamurthy et al. 2016). However, it remains unclear if spatially localized, optogenetic

62   activation of ERK and AKT activity allows for subcellular control of cellular outcomes.

63   In this study, we used optoRaf and optoAKT to specifically activate the Raf/MEK/ERK

64   and AKT signaling subcircuits, respectively. We found that both optoRaf and optoAKT activity

65   enhanced axon regeneration in the regeneration-potent class IV da (C4da) and the regeneration-

66   incompetent class III da (C3da) sensory neurons in *Drosophila* larvae, although optoRaf but not

67   optoAKT enhanced dendritic branching. Temporally programmed and spatially restricted light

68   stimulation showed that optoRaf and optoAKT differ in their signaling kinetics during

69   regeneration and that both allow spatially guided axon regrowth. Furthermore, using a

70   thermonociception based behavioral recovery assay, we found that optoRaf and optoAKT

71   activation led to effective axon regeneration as well as functional recovery after central nervous

72   system (CNS) injury. We note that most of previous optogenetic control of neural repair studies

73   were based on channelrhodopsion in *C. elegans* (Sun et al. 2014), mouse DRG culture (Park et al.

74   2015a) or motor neuron-schwann cell co-culture (Hyung et al. 2019). Another study used blue-

75   light activatable adenylyl cyclase bPAC to stimulate neural repair in mouse refractory axons

76   (Xiao et al. 2015). These work highlights the feasibility of using optogenetics to study neural

77   repair but did not pin down the exact downstream signaling cascade mediating neuronal repair.

78   Additionally, most studies focused on peripheral neurons that are endogenously regenerative.

79   Here, we specifically activated the ERK and AKT signaling pathways and performed a

80   comprehensive study of neural regeratnion in both peripheral nervous system (PNS) and CNS

81   neurons in live *Drosophila*. We envision that features provided by non-neuronal optogenetics,

82   including reversibility, functional delineation, and spatiotemporal control will lead to a better

83   understanding of the link between signaling kinetics and functional outcome of neurotrophic

84   signaling pathways during neuroregeneration.

85

86   **Results**

87   **Light enables reversible activation of the Raf/MEK/ERK and AKT signaling pathways**

88   To reversibly control the Raf/MEK/ERK and AKT signaling pathways, we constructed a single-

89   transcript optogenetic system using the p2A bicistronic construct that co-expresses fusion-

90   proteins with the N-terminus of cryptochrome-interacting basic-helix-loop-helix (CIBN) and the

91   photolyase homology region of cryptochrome 2 (CRY2PHR, abbreviated as CRY2 in this work).

92   Following a similar design of the optimized optoRaf (Krishnamurthy et al. 2016), we imporved

93　the previous optogenetic AKT system (Ong et al. 2016) with two tandom CIBNs (referred to as

94　optoAKT in this work) (Supplemental Fig. S1A). Consistent with previous studies, the association

95　of CIBN and CRY2 took about 1 second and the CIBN-CRY2 complex dissociated in the dark

96　within 10 minutes (Kennedy et al. 2010; Zhang et al. 2014). The fusion of Raf or AKT does not

97　affect the association and dissociation kinetics of CIBN and CRY2 and multiple cycles of CRY2-

98　CIBN association and dissociation can be triggered by alternating light-dark treatment

99　(Supplemental Fig. S1B-S1D, Movie S1, S3). Activation of optoRaf and optoAKT resulted in

100　nuclear translocation of ERK-EGFP (Fig. 1A, Movie S2) and nuclear export of FOXO3-EGFP

101　(Fig. 1B, Movie S4) resolved by live-cell fluorescence imaging, indicative of activation of the

102　ERK and AKT signaling pathways, respectively.

103　　　Western blot analysis on pERK (activated by optoRaf) in HEK293 cells showed that

104　pERK activity (Fig. 1C) increased within 10 min blue light stimulation and returned to the basal

105　level 30 min after the blue light was shut off (Fig. 1D). There was a slight decrease of pERK

106　activity upon optoRaf activation for over 10 min, likely due to a negative feedback, which has

107　been consistently observed in previous studies (Zhou et al. 2017). On the other hand, continuous

108　light illumination maintained a sustained activation of pCRY2-mCh-AKT (referred to as

109　optoAKT in this work) within an onset of 10 min (Fig. 1E). The inactivation kinetics of pAKT

110　was 30 min, similar to that of pERK (Fig. 1F, 1G). Note we use only the phosphorylated and

111　total forms of CRY2-mCh-AKT to quantify the light response of optoAKT because the

112　endogenous AKT does not respond to light.

113

114　**optoRaf and optoAKT do not show crosstalk activity at the pERK and pAKT level**

115   Binding of neurotrophins to their receptor activates multiple downstream signaling subcircuits

116   including the Raf/MEK/ERK, AKT, and phospholipase Cγ (PLCγ) pathways. Delineation of

117   signaling outcomes of individual subcircuits remains difficult with pharmacological assays given

118   the unpredictable off-targets of small-molecule drugs. We hypothesized that optoRaf and

119   optoAKT could delineate signaling outcomes because they bypass ligand binding and activate

120   the intracellular signaling pathway. To test this hypothesis, we probed phosphorylated proteins

121   including pERK, pAKT, and pPLCγ with WB analysis in response to light-mediated activation

122   of optoRaf and optoAKT. Results show that optoRaf activation does not increase pAKT and

123   pPLCγ (Fig. 1H, 1I). Similarly, optoAKT activation does not increase pERK or pPLCγ (Fig. 1H,

124   1I). Thus, at the ERK and AKT level, optoRaf and optoAKT do not show crosstalk activity in

125   mammalian cells.

126

127   **Activation of optoRaf but not optoAKT enhances PC12 cell neuritogenesis**

128   We verified that activation of optoRaf enhances PC12 cell neuritogenesis, which is consistent

129   with previous studies (Zhang et al. 2014; Krishnamurthy et al. 2016). The neuritogenesis ratio is

130   defined as the ratio between the number of transfected cells with at least one neurite longer than

131   the size of the cell body and the total number of transfected cells. Twenty-four hours of blue light

132   stimulation (0.2 mW/cm^2) increased the neuritogenesis ratio from the basal level (0.24 ± 0.04) to

133   0.52 ± 0.03 (Fig. 1J, 1L). Light-mediated activation of optoAKT, on the other hand, did not

134   increase the neuritogenesis ratio (0.23 ± 0.04 in the dark versus 0.20 ± 0.02 under light) (Fig. 1K,

135   1L). A membrane-targeted Raf1 (Raf1-GFP-CaaX) was used as a positive control, which caused

136   significant neurite outgrowth independent of light treatment (0.65 ± 0.01 in the dark versus 0.63

137   ± 0.01 under light). Expression of CIBN2-GFP-CaaX (without CRY2-Raf1), a negative control,

6

138   did not increase PC12 neurite outgrowth either in the dark (0.20 ± 0.02) or under light ($0.14 \pm$

139   0.01) (Fig. 1L).

140

141   **Activation of optoRaf but not optoAKT increases sensory neuron dendrite branching in fly**

142   **larvae**

143   To determine the efficacy of the optogenetic tools *in vivo*, we generated transgenic flies with

144   inducible expression of optoRaf (*UAS-optoRaf*) and optoAKT (*UAS-optoAKT*). We induced the

145   expression of the transgenes in a type of fly sensory neurons, the dendritic arborization (da)

146   neurons, which have been used extensively to study dendrite morphogenesis and remolding (Gao

147   et al. 1999; Grueber et al. 2002; Sugimura et al. 2003; Kuo et al. 2005; Williams and Truman

148   2005; Kuo et al. 2006; Williams et al. 2006; Parrish et al. 2007). Using the *pickpocket (ppk)-*

149   *Gal4*, we specifically expressed optoRaf in the class IV da (C4da) neurons, to test whether light

150   stimulation would activate the Raf/MEK/ERK pathway. At 72 hours after egg laying (h AEL),

151   wild-type (WT) and optoRaf-expressing larvae were anesthetized with ether and subjected to

152   wholefield continuous blue light for 5 min, while as a control, another transgenic group was

153   incubated in the dark. The larval body walls were then dissected and immunostained with the

154   pERK1/2 antibody, as a readout of the Raf/MEK/ERK pathway activation. We found that,

155   compared with the optoRaf-expressing larvae incubated in the dark and WT larvae, light

156   stimulation significantly increased the pERK signal in the cell body of C4da neurons in optoRaf-

157   expressing larvae (Fig. 2A), leading to 3.5-fold increase in fluorescence intensity (Fig. 2B).

158   Similarly, in C4da neurons expressing optoAKT, the 5-min blue light stimulation significantly

159   increased the fluorescence intensity of phospho-p70 S6 kinase (phospho-p70^{S6K}) (Fig. 2C, 2D),

160   which functions downstream of AKT (Lizcano et al. 2003; Miron et al. 2003). These results

7

161   collectively demonstrate that blue light is sufficient to activate the optogenetic effectors in flies

162   *in vivo*.

163   We next investigated if optoRaf or optoAKT activation would affect neural development

164   such as dendrite morphogenesis. We labeled C4da neurons with *ppk-CD4tdGFP* and

165   reconstructed the dendrites of the lateral C4da neurons – v'ada. Without light stimulation, the

166   dendrite complexity of neurons in transgenic larvae was comparable to that of WT (Fig. 2F, 2G).

167   However, optoRaf activation resulted in a significant increase in both total dendrite length and

168   branch number, while optoAKT activation exhibited a slight reduction in dendritic branching

169   (Fig. 2E-2G). These results confirm the possibility of independently activating the

170   Raf/MEK/ERK and AKT signaling pathways in flies with our optogenetic tools, prompting us to

171   test the feasibility of their *in vivo* applications, such as promoting axon regeneration with high

172   spatial and temporal resolution.

173

174   **Activation of optoRaf or optoAKT results in enhanced axon regeneration in the PNS**

175   Administration of neurotrophins to damaged peripheral neurons results in functional regeneration

176   of sensory axons into the adult spinal cord in rat (Ramer et al. 2000). Here, our photoactivatable

177   transgenic flies empower precise spatiotemporal control of the neurotrophic signaling in live

178   animals. To test whether light-mediated activation of the Raf/MEK/ERK or AKT signaling

179   subcircuits would also promote axon regrowth, we used a previously described *Drosophila* da

180   sensory neuron injury model (Song et al. 2012; Song et al. 2015). Da neurons have been shown

181   to possess distinct regeneration capabilities among different sub-cell types, and between the PNS

182   and CNS, resembling mammalian neurons (Song et al. 2012; Song et al. 2015). In particular, the

183   C4da neurons regenerate their axons robustly after peripheral injury, while the C3da neurons

184   largely fail to regrow. Moreover, the axon regeneration potential of C4da neurons is also

185   diminished after CNS injury. First, we asked whether optoRaf or optoAKT activation can

186   enhance axon regeneration in the regeneration-competent C4da neurons in the PNS. We severed

187   the axons of C4da neurons (labeled with *ppk-CD4tdGFP*) with a two-photo laser at 72 h AEL,

188   verified axon degeneration at 24 h after injury (AI) and assessed axon regeneration at 48 h AI. At

189   this time point, about 79% C4da neurons in WT showed obvious axon regrowth, and the

190   regeneration index (Song et al. 2012; Song et al. 2015), which refers to the increase in axon

191   length normalized to larval growth (Supplementary Fig. 2A, 2B, and Materials and Methods),

192   was 0.381 ± 0.066 (Fig. 3A-3C). Strikingly, C4da neurons expressing optoRaf or optoAKT

193   showed further enhanced regeneration potential in response to blue light, leading to a significant

194   increase in the regeneration index (*optoRaf*: 0.682 ± 0.115; *optoAKT*: 0.735 ± 0.078), while there

195   was no difference between WT and unstimulated transgenic flies (Fig. 3A-3C). In order to test

196   the potential synergy between optoRaf and optoAKT, we co-expressed both in C4da neurons.

197   While there is a slight increase in the regeneration percentage, activation of both ERK and AKT

198   pathways in the same neuron did not further increase the regeneration index (0.7387 ± 0.08390)

199   (Fig. 3A-3C). This suggests that these two subcircuits may share the same downstream

200   components in promoting axon regeneration. Alternatively, activation of the ERK or AKT

201   pathway by optogenetics may be strong enough to cause a saturation effect in C4da neurons axon

202   regeneration.

203   The light stimulation paradigm used in the aforementioned *in vivo* experiments was

204   constant blue light applied immediately after injury. We reason that intermittent light stimulation

205   may provide insights into the signaling kinetics *in vivo* and fine-tune axon regeneration dynamics.

206   Therefore, instead of constant blue light on, we delivered two sets of programmed light patterns

207   to injured larvae, 15 min on-15 min off or 15 min on-45 min off per cycle for 48 h (Fig. 3D). We

208   found that, for optoRaf-expressing C4da neurons, when the off-time was 15 min, the intermittent

209   light stimulation was sufficient to accelerate axon regrowth, with both the regeneration index

210   (0.6352 ± 0.09627) and regeneration percentage significantly increased compared to larvae

211   incubated in the dark (Fig. 3E, 3F). However, when the off-time was 45 min, the intermittent

212   light failed to promote axon regeneration (Fig. 3E, 3F), suggesting a threshold effect. On the

213   other hand, C4da neurons expressing optoAKT displayed a graded response: a moderate increase

214   of regeneration index (0.6278 ± 0.09801) in response to the 15 min on-15 min off light and a

215   smaller uptick to the 15 min on-45 min off light; both were less effective than the constant light

216   stimulation (Fig. 3E, 3F). These results suggest that although higher frequency of light

217   stimulation generally resulted in stronger regeneration potential in the transgenic flies, constant

218   light was not always required for maximum axon regeneration. Moreover, optoRaf and optoAKT

219   differ in their signaling kinetics during regeneration, showing a gated versus graded response,

220   respectively.

221   We next determined whether optoRaf or optoAKT activation would trigger regeneration

222   in C3da neurons, which are normally incapable of regrowth (Song et al. 2012). C3da neurons

223   were labeled with *19-12-Gal4, UAS-CD4tdGFP, repo-Gal80* and injured using the same

224   paradigm as C4da neurons. Compared to WT, which exhibited poor axon regeneration ability

225   demonstrated by the low regeneration percentage and the negative regeneration index (-0.03201

226   ± 0.02752) (Fig. 3G-3I), light stimulation significantly increased the regeneration index in

227   optoRaf- or optoAKT-expressing larvae to 0.1298 ± 0.04637 or 0.1354 ± 0.06161, respectively

228   (Fig. 3G-3I). These results indicate that optoRaf and optoAKT activation not only accelerates

229   axon regeneration but also converts regeneration cell-type specificity.

10

230

Spatial activation of optoRaf or optoAKT improves pathfinding of regenerating axons

While C4da neurons are known to possess the regenerative potential, it is unclear whether the regenerating axons navigate correctly. To address this question, we focused on v'ada – the lateral C4da neurons. Uninjured v'ada axons grow ventrally, showing a typical turn and then join the axon bundle with the ventral C4da neurons (Supplementary Fig. 2A). We found that their regenerating axons preferentially regrew away from the original ventral trajectory. More than 60% v'ada axons bifurcated and formed two branches targeting opposite directions (Fig. 4A, 4B white bar). In the majority cases in WT, the ventral branch, which extends towards the correct trajectory, regenerated less frequently than the dorsal branch, with 15% v'ada containing only the ventral branch (Fig. 4A, 4B black bar). One possibility is that the ventral branch encounters the injury site, which may retard its elongation. As a result, only a minority of regenerating axons are capable of finding the correct path. The poor pathfinding of regenerating axons was similar among WT and the transgenic larvae, regardless of whether incubated with whole-field light or in the dark (Fig. 4B). Thus, proper guidance of the regenerating axons towards the correct trajectory remained to be resolved.

We thus investigated whether spatially restricted activation of the neurotrophic signaling using our optogenetic system could guide the regenerating axons. To specifically enhance the regrowth of the ventral branch, we used a confocal microscope to focus the blue light (delivered by the 488 nm argon-ion laser) on the ventral branch for 5 min at 24 h AI. The lengths of both the ventral and dorsal branches were measured at 24 h AI and 48 h AI. We subtracted the increased dorsal branch length (Δdorsal) from the increased ventral branch length (Δventral), then divided that by the total increased length of these two branches (Fig. 4D). This value was

253   defined as the relative regeneration ratio. If the dorsal branch exhibited more regenerative

254   potential, the ratio would be negative; otherwise, it would be positive. Without light stimulation,

255   the relative regeneration ratio of the transgenic larvae (*optoRaf*: -0.6062 ± 0.1453; *optoAKT*: -

256   0.5530 ± 0.1011) was comparable to that of WT (-0.5786 ± 0.08229) (Fig. 4C, 4D), confirming

257   preferred regrowth of the dorsal branch. Strikingly, the 5-min local blue light stimulation

258   significantly increased the ratio in optoRaf- or optoAKT-expressing v'ada (*optoRaf*: 0.04762 ±

259   0.1123; *optoAK*T: -0.1725 ± 0.09560), while this transient stimulation resulted in no difference

260   in WT (-0.6018 ± 0.1290) (Fig. 4C, 4D). This result indicates that a single pulse of local light

261   stimulation was sufficient to lead to preferential regrowth of the ventral branch. Notably,

262   although whole-field light illumination could significantly promote axon regrowth, it failed to

263   increase the relative regeneration ratio in transgenic larvae (Con.on *optoRaf*: -0.7048 ± 0.1015;

264   Con. on *optoAKT*: -0.5517 ± 0.09644) (Fig. 4D), revealing the difference between activating the

265   neurotrophic signaling in a whole neuron and a single lesioned axon branch. On the other hand,

266   while a 5 min local light stimulation did not lead to an overall enhancement of axon regrowth, it

267   provided adequate guidance instructions for the regenerating axons to make the correct choice.

268

269   **Activation of optoRaf or optoAKT promotes axon regeneration and functional recovery in**

270   **the CNS**

271   Achieving functional axon regeneration after CNS injury remains a major challenge in neural

272   repair research. Motivated by the capacity of optoRaf and optoAKT to accelerate axon

273   regeneration in the PNS, we went on to determine whether they also show efficacy after CNS

274   injury. We focused on the axons of C4da neurons, which project into the ventral nerve cord

275   (VNC) and form a ladder-like structure. Each pair of axon bundles correspond to one body

276   segment in an anterior-posterior pattern (Fig. 5A) (Li et al., submitted). We injured the

277   abdominal A6 and A3 bundles by laser as previously described (Song et al. 2012) (Li et al.,

278   submitted) (Supplementary Fig. 3), and confirmed axon degeneration at 24 h AI (Fig. 5A). At 48

279   h AI, we found that axons began to extend from the retracted axon stem and towards the

280   commissure region. We defined a commissure segment as regenerated only when at least one

281   axon extended beyond the midline of the commissure region or joined into other intact bundles

282   (Supplementary Fig. 3). In WT, only 16% of lesioned commissure segments displayed obvious

283   signs of regrowth (Fig. 5A, 5B). To quantify the extent of regrowth, we measured the length of

284   the regrown axons and normalized that to the length of a commissure segment – regeneration

285   index (Supplementary Fig. 3, Materials and Methods). After light stimulation, the regeneration

286   indexes of the two transgenic lines (*optoRaf*: 5.375 ± 0.3391; *optoAKT*: 4.765 ± 0.4236) were

287   significantly increased compared with the WT control (2.643 ± 0.3050), and the percentage of

288   regenerating commissure segments also exhibited a mild increase in both optoRaf- and

289   optoAKT- expressing larvae (Fig. 5A-5C). On the other hand, there was no significant difference

290   between WT and the unstimulated transgenic flies (Fig. 5A-5C). This result suggests that both

291   signaling subcircuits reinforce C4da neuron axon regeneration in the CNS.

292   We then tested whether the axon regrowth in the CNS induced by optoRaf or optoAKT

293   activation leads to behavioral improvement. We utilized a recently established behavioral

294   recovery paradigm based on larval thermonociception (Fig. 6A, Materials and Methods) (Li et al.,

295   submitted). In brief, we injured the A7 and A8 C4da neuron axon bundles in the VNC, which

296   correspond to the A7 and A8 body segments in the periphery. We then assessed the nociceptive

297   behavior in these larvae in response to a 47 °C heat probe applied at the A7 or A8 segments at 24

298   and 48 h AI. Since C4da neurons are essential for thermonociception, injuring A7 and A8 axon

299   bundles in the VNC would lead to an impaired nociceptive response to the heat probe

300   specifically at body segments A7 and A8. Indeed, all the injured larvae exhibited diminished

301   response at 24 h AI, while the total score is approaching 3 in uninjured WT larvae (Fig. 6B). At

302   48 h AI, substantial recovery was observed in the two transgenic groups with light stimulation,

303   whereas WT showed very limited response and a low recovery percentage (Fig. 6B, 6C). Both

304   the response score and the percentage of larvae exhibiting behavioral recovery in these two

305   groups were more than twice as that of the WT, while the unstimulated groups were comparable

306   to WT. Altogether, these results demonstrate that our optogenetic system empowers ligand-free

307   and non-invasive control of the Raf/MEK/ERK and AKT pathways in flies, which not only

308   promote axon regeneration after injury but also benefit functional recovery, suggesting that the

309   regenerated axons may rewire and form functional synapses.

310

Discussion

312   Neurotrophins are known to activate Trk receptors and trigger the Ras/MEK/ERK, AKT, and

313   PLCγ pathways which are involved in cell survival, neural differentiation, axon and dendrite

314   growth and sensation (Bibel and Barde 2000; Huang and Reichardt 2001; Chao 2003; Cheng et

315   al. 2011; Joo et al. 2014). Here, we used optogenetic systems to achieve specific and reversible

316   activation of the neurotrophin subcircuits including the Raf/MEK/ERK (via optoRaf) and AKT

317   (via optoAKT) signaling pathways. We further verified that optoRaf and optoAKT did not show

318   crosstalk at the level of phosphorylated ERK and AKT proteins, and activation of optoRaf but

319   not optoAKT promoted PC12 cell differentiation.

320   After spinal cord injury, the synthesis of neurotrophins is elevated to support axon

321   regrowth (Cho et al. 1998; Hayashi et al. 2000; Fukuoka et al. 2001; Fang et al. 2017). AKT

14

322   signaling, which functions downstream of Trk receptors, was reported to accelerate axon

323   regeneration in fly and mammals (Song et al. 2012; Guo et al. 2016; Miao et al. 2016). However,

324   the role of Raf/MEK/ERK signaling played during nerve repair is controversial. Although some

325   studies revealed that ERK is involved in axon extension, others suggested that ERK activation

326   impedes axon regeneration and functional recovery (Markus et al. 2002; Huang et al. 2017;

327   Cervellini et al. 2018). To specifically evaluate the efficacy of Raf/MEK/ERK and AKT

328   signaling in promoting axon regeneration, we generated fly strains with tissue-specific

329   expression of optoRaf or optoAKT and found that light stimulation was sufficient to activate the

330   corresponding downstream components in fly larvae *in vivo*. Consistent with previous studies

331   (He and Jin 2016), we found that AKT activation resulted in significantly increased axon

332   regeneration in C4da neurons as well as the regeneration-incompetent C3da neurons.

333   Interestingly, we found that C4da and C3da neurons expressing optoRaf also exhibited greater

334   regeneration potential in response to light stimulation. This result also corroborates with a

335   previous finding that activated B-RAF signaling enables axon regeneration in the mammalian

336   CNS (O'Donovan et al. 2014). We speculate that the differential outcomes of ERK activation on

337   axon regeneration may be due to the different injury models used, and the strength and cell type

338   origin of ERK signaling.

339   The regenerative capacity varies significantly among different neuronal subtypes, as well

340   as the PNS and CNS. Although the administration of neurotrophins enhances axon regeneration

341   in peripheral neurons, its capacity to promote functional regeneration in the CNS is limited, in

342   part due to the inaccessibility of neurotrophins to reach injured axons (physical barrier) (Silver

343   and Miller 2004; Yiu and He 2006) and innate inactivation of the regenerating program in CNS

344   (Lu et al. 2014). OptoRaf and optoAKT could be used to address both issues by direct delivery

345   of light (rather than ligand) to reactivate the regenerating program and thereby significantly

346   increase neural regeneration in the CNS as well. We further showed that activation of the

347   Raf/MEK/ERK or AKT subcircuit was capable of improving behavioral performance in fly

348   larvae, suggesting that it may promote synapse regeneration leading to functional recovery.

349   Ineffective functional recovery at least partially results from the inappropriate pathfinding

350   of the regenerative neurons. As shown in this study, the majority of regenerating C4da neuron

351   axons preferentially grew away from their original trajectory. We surprisingly found that

352   delivering a 5-min light stimulation to the ventral branch, which extended towards the correct

353   direction, was sufficient to convey guidance instructions and increase the preferential elongation

354   of the ventral branch against the dorsal branch. Correct guidance cannot be achieved by whole-

355   body administration of pharmacological reagents. Similarly, when casting blue light on the

356   whole transgenic larvae, light stimulation must be given at a high frequency to promote axon

357   regrowth (there is a threshold for the light off-time), and the dorsal branch extension was also

358   dominant in this case. This result highlights the importance and necessity of restricted activation

359   of neurotrophic signaling. Indeed, the strength and location of Raf/MEK/ERK and AKT

360   activation during axon regeneration may be important to the functional consequences. Notably,

361   although the transient restricted stimulation likely affects the decision-making of the growth cone

362   at the branching point, constant light is still required to increase overall axon regeneration.

363   Neurotrophins are engaged in a variety of important cellular processes, and their

364   physiological concentration is essential for the normal function of both neurons and non-

365   neuronal cells (Rose et al. 2003; Xiao et al. 2010; Poyhonen et al. 2019). Despite exhibiting

366   substantial efficacy for enhancing nerve regeneration, neurotrophin-based therapeutic

367   applications have been confronted with a number of obstacles such as their nociceptive effects

368   and lack of strategy for localized signaling activation (Aloe et al. 2012; Mitre et al. 2017; Mahar

369   and Cavalli 2018; Sung et al. 2019). OptoRaf and optoAKT aim to improve neurotrophin

370   signaling outcomes by preferentially activating the neuroregenerative program and enabling

371   spatiotemporal control. Our systems offer insights into the ERK and AKT subcircuits and

372   delineate their differential roles downstream of neurotrophin activation, as evidenced by the

373   distinct functional outcomes of Raf/MEK/ERK and AKT signaling in several aspects. First, ERK

374   signaling promoted PC12 cell neuritogenesis, which was not induced by AKT activation. Second,

375   elevated ERK activity significantly increased dendritic complexity, while on the contrary, AKT

376   activation led to decreased dendrite branching. Third, after injury, C4da neurons expressing

377   optoRaf and optoAKT responded differently to intermitted light stimulation, suggesting that their

378   strength and activation duration is differentially gauged during axon regeneration. These

379   collectively suggest that, since Raf could be activated by membrane translocation as well as

380   dimerization, CRY2 oligomerization could further lead to a more potent Raf. This multimodal

381   activation mechanism may render that a threshold of optoRaf can be reached so that a saturated

382   ERK activation could be achieved. On the other hand, AKT activation does not depend on

383   dimerization and may display a graded response. As a result, optoAKT activates the AKT

384   pathway in a dose-dependent manner and may not recapitulate the maximan activation of AKT.

385   This work provides a proof-of-principle to use optogenetics to accelerate and navigate axon

386   regeneration in mammalian injury models. Besides spatiotemporal control of the neurotrophic

387   signaling, optoRaf and optoAKT allow for finetuning of the signaling activity with programmed

388   light pattern during axon regeneration. Follow-up studies are warranted to determine how

389   Raf/MEK/ERK and AKT subcircuits are involved in each process of nerve repair, including

390   lesioned axon degeneration, regenerating axon initiation and extension, and the formation of new

391 synapses and remyelination in mammals. Understanding the machinery will, in turn, allow better

392 utilization and development of the optogenetic systems. Although intact optogenetics in larger

393 mammals is limited by the poor penetration depth of blue light (less than 1 mm), we are excited

394 to witness the rapid progress in implantable, wireless µLED devices (Jeong et al. 2015; Park et al.

395 2015b) and the integration of optogenetics with long-wavelength responsive nanomaterials such

396 as the upconversion nanoparticles (He et al. 2015; Wu et al. 2016; Chen et al. 2018), both of

397 which would facilitate precise delivery of light stimulation.

398

399 **Materials and Methods**

400 **Fly stocks**

401 *19-12-Gal4* (Xiang et al. 2010), *reop-Gal80* (Awasaki et al. 2008), *ppk-CD4-tdGFP* (Han et al.

402 2011), and *ppk-Gal4* (Han et al. 2011) have been previously described. To generate the *UAS-*

403 *optoRaf and UAS-optoAKT* stocks, the entire coding sequences were cloned into the pACU2

404 vector, and the constructs were then injected (Rainbow Transgenic Flies, Inc). Randomly

405 selected male and female larvae were used. Analyses were not performed blind to the conditions

406 of the experiments. The experimental procedures have been approved by the Institutional

407 Biosafety Committee (IBC) at the Children's Hospital of Philadelphia.

408

409 **Sensory axon lesion in *Drosophila***

410 Da neuron axon lesion and imaging in the PNS was performed in live fly larvae as previously

411 described (Song et al. 2012; Stone et al. 2014; Song et al. 2015). VNC injury was performed as

412 previously described (Song et al. 2012) (Li et al., submitted). In brief, A3 and A6 axon bundles

413 in the VNC were ablated with a focused 930-nm two-photon laser and full degeneration around

18

414   the commissure junction was confirmed 24 h AI. At 48 h AI, axon regeneration of these two

415   commissure segments were assayed independently of each other (Supplementary Fig. 3).

416

417   **Quantitative analyses of sensory axon regeneration in flies**

418   Quantification was performed as previously described (Song et al. 2012; Song et al. 2015).

419   Briefly, for axon regeneration in the PNS, we used "regeneration percentage", which depicts the

420   percent of regenerating axons among all the axons that were lesioned; "regeneration index",

421   which was calculated as an increase of "axon length"/"distance between the cell body and the

422   axon converging point (DCAC)" (Supplementary Fig. 2A, 2B). An axon was defined as

423   regenerating only when it obviously regenerated beyond the retracted axon stem, and this was

424   independently assessed of the other parameters. The regeneration parameters from various

425   genotypes were compared to that of the WT if not noted otherwise, and only those with

426   significant differences were labeled with the asterisks. For VNC injury, the increased length of

427   each axon regrowing beyond the lesion sites was measured and added together. To calculate the

428   regeneration index, the sum was then divided by the distance between A4 and A5 axon bundles

429   (Supplementary Fig. 3). Regeneration percentage was assessed independently of the regeneration

430   index. A commissure segment was defined as regenerated only when at least one regenerating

431   axon passed the midline of the commissure region or joined into other intact bundles

432   (Supplementary Fig. 3).

433

434   **Live imaging in flies**

435   Live imaging was performed as described (Emoto et al. 2006; Parrish et al. 2007). Embryos were

436   collected for 2-24 hours on yeasted grape juice agar plates and were aged at 25 °C or room

437 temperature. At the appropriate time, a single larva was mounted in 90% glycerol under

438 coverslips sealed with grease, imaged using a Zeiss LSM 880 microscope, and returned to grape

439 juice agar plates between imaging sessions.

440

441 **Behavioral assay**

442 The behavioral test was performed to detect functional recovery after VNC injury as described

443 (Li et al., submitted). A7 and A8 C4da neuron axon bundles in the VNC, which correspond to

444 the A7 and A8 body segments in the periphery, were injured with laser (Fig. 6A). Since C4da

445 neurons are essential for thermonociception, such lesion results in impaired nociceptive response

446 to noxious heat at body segments A7 and A8. We assessed larva nociceptive behavior in

447 response to a 47 °C heat probe at 24 and 48 h AI. At each time point, the larva was subjected to

448 three consecutive trials, separated by 15 seconds (s). In each trial, the heat probe was applied at

449 the A7 and A8 body segments for 5 s. If the larva produced head rolling behavior for more than 2

450 cycles, it would be scored as "1", otherwise "0" (Fig. 6A). The scores of the three trials were

451 combined and the total score at 24 h AI was used to determine whether A7 and A8 bundles were

452 successfully ablated. A larva was defined as recovered only when its total score was below 1 at

453 24 h AI but increased to 2 or 3 at 48 h AI. Those failed to exhibit such improvement at 48 h AI

454 were defined as unrecovered. All the injured larvae exhibited normal nociceptive responses when

455 the same heat probe was applied at the A4 or A5 body segment at 24 h AI.

456

457 **Immunohistochemistry**

458 Third instar larvae or cultured neurons were fixed according to standard protocols. The following

459 antibodies were used: rabbit anti-Phospho-p44/42 MAPK (Erk1/2) (Thr202/Tyr204) (4370,

460   1:100, Cell Signaling), rabbit anti-Phospho-*Drosophila* p70 S6 Kinase (Thr398) (9209S, 1:200,

461   Cell Signaling) and fluorescence-conjugated secondary antibodies (1:1000, Jackson

462   ImmunoResearch).

463

464   **Cell culture and transfection**

465   HEK293T cells were cultured in DMEM medium supplemented with 10% FBS, and 1x

466   Penicillin-Streptomycin solution (complete medium). Cultures were maintained in a standard

467   humidified incubator at 37 °C with 5% CO_2. For western blots, 800 ng of DNA were combined

468   with 2.4 µL Turbofect in 80 µL of serum-free DMEM. The transfection mixtures were incubated

469   at room temperature for 20 minutes prior to adding to cells cultured in 35 mm dishes with 2 mL

470   complete medium. The transfection medium was replaced with 2 mL serum-free DMEM

471   supplemented with 1× Penicillin-Streptomycin solution after 3 hours of transfection to starve

472   cells overnight. PC12 cells were cultured in F12K medium supplemented with 15% horse serum,

473   2.5% FBS, and 1× Penicillin-Streptomycin solution. (For PC12 neuritogenesis assays, 2400 ng

474   of DNA were combined with 7.2 mL of Turbofect in 240 mL of serum-free F12K. The

475   transfection medium was replaced with 2 mL complete medium after 3 hours of transfection to

476   recover cells overnight.). Twenty-four hours after recovery in high-serum F12K medium [15%

477   horse serum + 2.5% fetal bovine serum (FBS)], the cell culture was exchanged to a low-serum

478   medium (1.5% horse serum + 0.25% FBS) to minimize the base-level ERK activation induced

479   by serum.

480

481   **Optogenetic stimulation for cell culture**

482   For Western blot analysis, transfected and serum-starved cells were illuminated for different time

483   using a home-built blue LED light box emitting at 0.5 mW/cm^2. For PC12 cell neuritogenesis

484   assay, PC12 cells were illuminated at 0.2 mW/cm^2 for 24 h with the light box placed in the

485   incubator.

486

487   **Optogenetic stimulation for fly**

488   The whole optogenetics setup is modified from previous work (Kaneko et al. 2017). Larvae were

489   grown in regular brown food at 25 °C in 12 h-12 h light-dark cycle. At 72 h AEL, early 3rd

490   instar larvae were transferred from food, anesthetized with ether for axotomy. After recovery in

491   regular grape juice agar plates, larvae were kept in the dark or under blue light stimulation

492   thereafter. A 470 nm blue LED (LUXEON Rebel LED) was set over the grape-agar plate for

493   stimulation. The LED was mounted on a 10 mm square coolbase and 50 mm square × 25mm

494   high alpha heat sink and set under circular beam optic with integrated legs for parallel even light.

495   The light pattern was programmed with BASIC Stamp 2.0 microcontroller and buckpuck DC

496   driver (LUXEON, 700 mA, externally dimmable).

497   Local light stimulation was delivered by a 488 nm argon-ion laser using a Zeiss LSM 880

498   microscope. At 24 h AI, larvae were anesthetized and C4da neurons were imaged with a

499   confocal microscope. For lesioned axons that bifurcated and formed two branches, we focused

500   the laser beam (at 15% laser power) on the ventral branch for 5 min. The larva was then returned

501   to grape juice agar plates and imaged again at 48 h AI to assess the increased length of each

502   branch.

503

504   **Live cell imaging**

505   For the light-induced membrane recruitment assay, BHK-21 cells were co-transfected with

506   optoRaf or optoAKT. Fluorescence imaging of the transfected cells was carried out using a

507   confocal microscope (Zeiss LSM 700). GFP fluorescence was excited by a 488-nm laser beam;

508   mCherry fluorescence was excited by a 555-nm laser beam. Excitation beams were focused via a

509   40× oil objective (Plan-Neofluar NA 1.30). Ten pulsed 488-nm and 555-nm excitation were

510   applied for each membrane recruitment experiment. CRY2-CIBN binding induced by 488-nm

511   light was monitored by membrane recruitment of CRY2-mCherry-Raf1 (for optoRaf) or CRY2-

512   mCherry-AKT (for optoAKT) to the CIBN-CIBN-GFP-CaaX-anchored plasma membrane. The

513   powers after the objective for 488-nm and 555-nm laser beam are approximately 40 µW and 75

514   µW, respectively. Alternatively, an epi-illumination fluorescence microscope (Leica DMI8)

515   equipped with a 100× objective (HCX PL FLUOTAR 100×/1.30 oil) and a light-emitting diode

516   illuminator (SOLA SE II 365) was used for the CRY2-mCherry-Raf1 membrane translocation

517   assay. Neurite outgrowth of PC12 cells was imaged using an epi-illumination fluorescence

518   microscope (Leica DMI8) equipped with 10× (PLAN 10×/0.25) and 40× (HCXPL FL L 40×/0.6)

519   objectives. Fluorescence from GFP was detected using the GFP filter cube (Leica, excitation

520   filter 472/30, dichroic mirror 495, and emission filter 520/35); fluorescence from mCherry was

521   detected using the Texas Red filter cube (Leica, excitation filter 560/40, dichroic mirror 595, and

522   emission filter 645/75).

523

524   **Western Blot**

525   Cells were washed once with 1 mL cold DPBS and lysed with 100 µL cold lysis buffer (RIPA +

526   protease/phosphatase cocktail). Lysates were centrifuged at 17,000 RCF, 4 °C for 10 minutes to

527   pellet cell debris. Purified lysates were normalized using Bradford reagent. Normalized samples

528   were mixed with LDS buffer and loaded onto 10% or 12% polyacrylamide gels. SDS-PAGE was

529   performed at room temperature with a cold water bath. Samples were transferred to PVDF

530   membranes at 30 V 4 °C overnight or 80 V for 90 minutes. Membranes were blocked in 5%

531   BSA/TBST for 1 hour at room temperature and probed with the primary and secondary

532   antibodies according to company guidelines. Membranes were incubated with ECL substrate and

533   imaged using a Bio-Rad ChemiDoc XRS chemiluminescence detector. Signal intensity analysis

534   was performed by ImageJ.

535

536   **Statistical Analysis**

537   No statistical methods were used to pre-determine sample sizes but our sample sizes are similar

538   to those reported in previous publications (Song et al. 2012; Song et al. 2015), and the statistical

539   analyses were done afterward without interim data analysis. Data distribution was assumed to be

540   normal but this was not formally tested. All data were collected and processed randomly. Each

541   experiment was successfully reproduced at least three times and was performed on different days.

542   The values of ''N'' (sample size) are provided in the figure legends. Data are expressed as mean

543   ± SEM in bar graphs, if not mentioned otherwise. No data points were excluded. Two-tailed

544   unpaired Student's t-test was performed for comparison between two groups of samples. One-

545   way ANOVA followed by multiple comparison test was performed for comparisons among three

546   or more groups of samples. Two-way ANOVA followed by multiple comparison test was

547   performed for comparisons between two or more curves. Fisher's exact test was used to compare

548   the percentage. Statistical significance was assigned, $*P < 0.05$, $**P < 0.01$, $***P < 0.001$.

549

550   **Acknowledgments**

553

554   Author Contributions

555   Y.S., K.Z. and Q.W. conceived the experimental design. Q.W., H.F., F.L., S.S.S, and V.V.K.

556   conducted the experiments. Q. W. and H. F. analyzed the data. Q.W., H.F., Y.S., and K.Z.

557   prepared the manuscript and figures.

558

559   Conflict of interest

560   The authors declare no conflict of interest.

561

562   References

563   Aloe L, Rocco ML, Bianchi P, Manni L. 2012. Nerve growth factor: from the early discoveries

564   to the potential clinical use. *J Transl Med* **10**.

565   Awasaki T, Lai SL, Ito K, Lee T. 2008. Organization and postembryonic development of glial

566   cells in the adult central brain of Drosophila. *J Neurosci* **28**: 13742-13753.

567   Bibel M, Barde YA. 2000. Neurotrophins: key regulators of cell fate and cell shape in the

568   vertebrate nervous system. *Genes Dev* **14**: 2919-2937.

569   Cervellini I, Galino J, Zhu N, Allen S, Birchmeier C, Bennett DL. 2018. Sustained MAPK/ERK

570   Activation in Adult Schwann Cells Impairs Nerve Repair. *J Neurosci* **38**: 679-690.

571   Chao MV. 2003. Neurotrophins and their receptors: A convergence point for many signalling

572   pathways. *Nature Reviews Neuroscience* **4**: 299-309.

573 Chen S, Weitemier AZ, Zeng X, He L, Wang X, Tao Y, Huang AJY, Hashimotodani Y, Kano M,

574   Iwasaki H et al. 2018. Near-infrared deep brain stimulation via upconversion

575   nanoparticle-mediated optogenetics. *Science* **359**: 679-684.

576 Cheng PL, Song AH, Wong YH, Wang S, Zhang X, Poo MM. 2011. Self-amplifying autocrine

577   actions of BDNF in axon development. *Proc Natl Acad Sci U S A* **108**: 18430-18435.

578 Cho HJ, Kim JK, Park HC, Kim JK, Kim DS, Ha SO, Hong HS. 1998. Changes in brain-derived

579   neurotrophic factor immunoreactivity in rat dorsal root ganglia, spinal cord, and gracile

580   nuclei following cut or crush injuries. *Exp Neurol* **154**: 224-230.

581 Dagliyan O, Hahn KM. 2019. Controlling protein conformation with light. *Curr Opin Struct Biol*

582   **57**: 17-22.

583 Dine E, Gil AA, Uribe G, Brangwynne CP, Toettcher JE. 2018. Protein Phase Separation

584   Provides Long-Term Memory of Transient Spatial Stimuli. *Cell Syst* **6**: 655-663.

585 Emoto K, Parrish JZ, Jan LY, Jan YN. 2006. The tumour suppressor Hippo acts with the NDR

586   kinases in dendritic tiling and maintenance. *Nature* **443**: 210-213.

587 Fang H, Liu C, Yang M, Li H, Zhang F, Zhang W, Zhang J. 2017. Neurotrophic factor and Trk

588   signaling mechanisms underlying the promotion of motor recovery after acute spinal cord

589   injury in rats. *Exp Ther Med* **14**: 652-656.

590 Fukuoka T, Kondo E, Dai Y, Hashimoto N, Noguchi K. 2001. Brain-derived neurotrophic factor

591   increases in the uninjured dorsal root ganglion neurons in selective spinal nerve ligation

592   model. *J Neurosci* **21**: 4891-4900.

593 Gao FB, Brenman JE, Jan LY, Jan YN. 1999. Genes regulating dendritic outgrowth, branching,

594   and routing in Drosophila. *Genes & development* **13**: 2549-2561.

595 Goglia AG, Toettcher JE. 2019. A bright future: optogenetics to dissect the spatiotemporal

596   control of cell behavior. *Curr Opin Chem Biol* **48**: 106-113.

597 Grueber WB, Jan LY, Jan YN. 2002. Tiling of the Drosophila epidermis by multidendritic

598   sensory neurons. *Development* **129**: 2867-2878.

599 Guo X, Snider WD, Chen B. 2016. GSK3beta regulates AKT-induced central nervous system

600   axon regeneration via an eIF2Bepsilon-dependent, mTORC1-independent pathway. *Elife*

601   **5**: e11903.

602 Han C, Jan LY, Jan YN. 2011. Enhancer-driven membrane markers for analysis of

603   nonautonomous mechanisms reveal neuron-glia interactions in Drosophila. *Proc Natl*

604   *Acad Sci U S A* **108**: 9673-9678.

605 Hayashi M, Ueyama T, Nemoto K, Tamaki T, Senba E. 2000. Sequential mRNA expression for

606   immediate early genes, cytokines, and neurotrophins in spinal cord injury. *J Neurotrauma*

607   **17**: 203-218.

608 He L, Zhang YW, Ma GL, Tan P, Li ZJ, Zang SB, Wu X, Jing J, Fang SH, Zhou LJ et al. 2015.

609   Near-infrared photoactivatable control of Ca2+ signaling and optogenetic

610   immunomodulation. *Elife* **4**.

611 He Z, Jin Y. 2016. Intrinsic Control of Axon Regeneration. *Neuron* **90**: 437-451.

612 Huang EJ, Reichardt LF. 2001. Neurotrophins: roles in neuronal development and function.

613   *Annu Rev Neurosci* **24**: 677-736.

614 Huang H, Liu H, Yan R, Hu M. 2017. PI3K/Akt and ERK/MAPK Signaling Promote Different

615   Aspects of Neuron Survival and Axonal Regrowth Following Rat Facial Nerve Axotomy.

616   *Neurochem Res* **42**: 3515-3524.

617   Hyung S, Lee SR, Kim YJ, Bang S, Tahk D, Park JC, Suh JF, Jeon NL. 2019. Optogenetic

618   neuronal stimulation promotes axon outgrowth and myelination of motor neurons in a

619   three-dimensional motor neuron-Schwann cell coculture model on a microfluidic biochip.

620   *Biotechnol Bioeng* **116**: 2425-2438.

621   Jeong JW, McCall JG, Shin G, Zhang Y, Al-Hasani R, Kim M, Li S, Sim JY, Jang KI, Shi Y et

622   al. 2015. Wireless Optofluidic Systems for Programmable In Vivo Pharmacology and

623   Optogenetics. *Cell* **162**: 662-674.

624   Johnson HE, Toettcher JE. 2018. Illuminating developmental biology with cellular optogenetics.

625   *Curr Opin Biotechnol* **52**: 42-48.

626   Joo W, Hippenmeyer S, Luo L. 2014. Neurodevelopment. Dendrite morphogenesis depends on

627   relative levels of NT-3/TrkC signaling. *Science* **346**: 626-629.

628   Kaneko T, Macara AM, Li R, Hu Y, Iwasaki K, Dunnings Z, Firestone E, Horvatic S, Guntur A,

629   Shafer OT et al. 2017. Serotonergic Modulation Enables Pathway-Specific Plasticity in a

630   Developing Sensory Circuit in Drosophila. *Neuron* **95**: 623-638.

631   Kennedy MJ, Hughes RM, Peteya LA, Schwartz JW, Ehlers MD, Tucker CL. 2010. Rapid blue-

632   light-mediated induction of protein interactions in living cells. *Nat Methods* **7**: 973-975.

633   Khamo JS, Krishnamurthy VV, Chen Q, Diao J, Zhang K. 2019. Optogenetic Delineation of

634   Receptor Tyrosine Kinase Subcircuits in PC12 Cell Differentiation. *Cell Chem Biol* **26**:

635   400-410

636   Khamo JS, Krishnamurthy VV, Sharum SR, Mondal P, Zhang K. 2017. Applications of

637   Optobiology in Intact Cells and Multicellular Organisms. *J Mol Biol* **429**: 2999-3017.

638　Krishnamurthy VV, Khamo JS, Mei W, Turgeon AJ, Ashraf HM, Mondal P, Patel DB, Risner N,

639　　　Cho EE, Yang J et al. 2016. Reversible optogenetic control of kinase activity during

640　　　differentiation and embryonic development. *Development* **143**: 4085-4094.

641　Kuo CT, Jan LY, Jan YN. 2005. Dendrite-specific remodeling of Drosophila sensory neurons

642　　　requires matrix metalloproteases, ubiquitin-proteasome, and ecdysone signaling.

643　　　*Proceedings of the National Academy of Sciences of the United States of America* **102**:

644　　　15230-15235.

645　Kuo CT, Zhu S, Younger S, Jan LY, Jan YN. 2006. Identification of E2/E3 ubiquitinating

646　　　enzymes and caspase activity regulating Drosophila sensory neuron dendrite pruning.

647　　　*Neuron* **51**: 283-290.

648　Kyung T, Lee S, Kim JE, Cho T, Park H, Jeong YM, Kim D, Shin A, Kim S, Baek J et al. 2015.

649　　　Optogenetic control of endogenous Ca(2+) channels in vivo. *Nat Biotechnol* **33**: 1092-

650　　　1096.

651　Leopold AV, Chernov KG, Verkhusha VV. 2018. Optogenetically controlled protein kinases for

652　　　regulation of cellular signaling. *Chem Soc Rev*.

653　Liu BP, Cafferty WB, Budel SO, Strittmatter SM. 2006. Extracellular regulators of axonal

654　　　growth in the adult central nervous system. *Philos Trans R Soc Lond B Biol Sci* **361**:

655　　　1593-1610.

656　Liu K, Tedeschi A, Park KK, He Z. 2011. Neuronal intrinsic mechanisms of axon regeneration.

657　　　*Annu Rev Neurosci* **34**: 131-152.

658　Lizcano JM, Alrubaie S, Kieloch A, Deak M, Leevers SJ, Alessi DR. 2003. Insulin-induced

659　　　Drosophila S6 kinase activation requires phosphoinositide 3-kinase and protein kinase B.

660　　　*Biochem J* **374**: 297-306.

661   Lu Y, Belin S, He Z. 2014. Signaling regulations of neuronal regenerative ability. *Curr Opin*

662   *Neurobiol* **27**: 135-142.

663   Ma G, Liu J, Ke Y, Liu X, Li M, Wang F, Han G, Huang Y, Wang Y, Zhou Y. 2018.

664   Optogenetic Control of Voltage-Gated Calcium Channels. *Angew Chem Int Ed Engl* **57**:

665   7019-7022.

666   Mahar M, Cavalli V. 2018. Intrinsic mechanisms of neuronal axon regeneration. *Nat Rev*

667   *Neurosci* **19**: 323-337.

668   Markus A, Zhong J, Snider WD. 2002. Raf and akt mediate distinct aspects of sensory axon

669   growth. *Neuron* **35**: 65-76.

670   Marshall CJ. 1995. Specificity of receptor tyrosine kinase signaling: transient versus sustained

671   extracellular signal-regulated kinase activation. *Cell* **80**: 179-185.

672   Miao L, Yang L, Huang H, Liang F, Ling C, Hu Y. 2016. mTORC1 is necessary but mTORC2

673   and GSK3beta are inhibitory for AKT3-induced axon regeneration in the central nervous

674   system. *Elife* **5**: e14908.

675   Miron M, Lasko P, Sonenberg N. 2003. Signaling from Akt to FRAP/TOR targets both 4E-BP

676   and S6K in Drosophila melanogaster. *Mol Cell Biol* **23**: 9117-9126.

677   Mitre M, Mariga A, Chao MV. 2017. Neurotrophin signalling: novel insights into mechanisms

678   and pathophysiology. *Clin Sci* **131**: 13-23.

679   Motta-Mena LB, Reade A, Mallory MJ, Glantz S, Weiner OD, Lynch KW, Gardner KH. 2014.

680   An optogenetic gene expression system with rapid activation and deactivation kinetics.

681   *Nat Chem Biol* **10**: 196-202.

682 O'Donovan KJ, Ma K, Guo H, Wang C, Sun F, Han SB, Kim H, Wong JK, Charron J, Zou H et

683 al. 2014. B-RAF kinase drives developmental axon growth and promotes axon

684 regeneration in the injured mature CNS. *J Exp Med* **211**: 801-814.

685 Ong Q, Guo S, Duan L, Zhang K, Collier EA, Cui B. 2016. The Timing of Raf/ERK and AKT

686 Activation in Protecting PC12 Cells against Oxidative Stress. *PLoS One* **11**: e0153487.

687 Park KK, Liu K, Hu Y, Smith PD, Wang C, Cai B, Xu B, Connolly L, Kramvis I, Sahin M et al.

688 2008. Promoting axon regeneration in the adult CNS by modulation of the PTEN/mTOR

689 pathway. *Science* **322**: 963-966.

690 Park S, Koppes RA, Froriep UP, Jia X, Achyuta AK, McLaughlin BL, Anikeeva P. 2015a.

691 Optogenetic control of nerve growth. *Sci Rep* **5**: 9669.

692 Park SI, Brenner DS, Shin G, Morgan CD, Copits BA, Chung HU, Pullen MY, Noh KN,

693 Davidson S, Oh SJ et al. 2015b. Soft, stretchable, fully implantable miniaturized

694 optoelectronic systems for wireless optogenetics. *Nat Biotechnol* **33**: 1280-1286.

695 Parrish JZ, Emoto K, Kim MD, Jan YN. 2007. Mechanisms that regulate establishment,

696 maintenance, and remodeling of dendritic fields. *Annu Rev Neurosci* **30**: 399-423.

697 Poyhonen S, Er S, Domanskyi A, Airavaara M. 2019. Effects of Neurotrophic Factors in Glial

698 Cells in the Central Nervous System: Expression and Properties in Neurodegeneration

699 and Injury. *Front Physiol* **10**: 486.

700 Ramer MS, Priestley JV, McMahon SB. 2000. Functional regeneration of sensory axons into the

701 adult spinal cord. *Nature* **403**: 312-316.

702 Rose CR, Blum R, Pichler B, Lepier A, Kafitz KW, Konnerth A. 2003. Truncated TrkB-T1

703 mediates neurotrophin-evoked calcium signalling in glia cells. *Nature* **426**: 74-78.

704   Schwab ME, Strittmatter SM. 2014. Nogo limits neural plasticity and recovery from injury. *Curr*

705   *Opin Neurobiol* **27**: 53-60.

706   Shin Y, Berry J, Pannucci N, Haataja MP, Toettcher JE, Brangwynne CP. 2017. Spatiotemporal

707   Control of Intracellular Phase Transitions Using Light-Activated optoDroplets. *Cell* **168**:

708   159-171 e114.

709   Silver J, Miller JH. 2004. Regeneration beyond the glial scar. *Nat Rev Neurosci* **5**: 146-156.

710   Song Y, Ori-McKenney KM, Zheng Y, Han C, Jan LY, Jan YN. 2012. Regeneration of

711   Drosophila sensory neuron axons and dendrites is regulated by the Akt pathway

712   involving Pten and microRNA bantam. *Genes Dev* **26**: 1612-1625.

713   Song Y, Sretavan D, Salegio EA, Berg J, Huang X, Cheng T, Xiong X, Meltzer S, Han C,

714   Nguyen TT et al. 2015. Regulation of axon regeneration by the RNA repair and splicing

715   pathway. *Nat Neurosci* **18**: 817-825.

716   Stone MC, Albertson RM, Chen L, Rolls MM. 2014. Dendrite injury triggers DLK-independent

717   regeneration. *Cell reports* **6**: 247-253.

718   Sugimura K, Yamamoto M, Niwa R, Satoh D, Goto S, Taniguchi M, Hayashi S, Uemura T. 2003.

719   Distinct developmental modes and lesion-induced reactions of dendrites of two classes of

720   Drosophila sensory neurons. *The Journal of neuroscience : the official journal of the*

721   *Society for Neuroscience* **23**: 3752-3760.

722   Sun F, He Z. 2010. Neuronal intrinsic barriers for axon regeneration in the adult CNS. *Curr Opin*

723   *Neurobiol* **20**: 510-518.

724   Sun L, Shay J, McLoed M, Roodhouse K, Chung SH, Clark CM, Pirri JK, Alkema MJ, Gabel

725   CV. 2014. Neuronal Regeneration in C. elegans Requires Subcellular Calcium Release by

726   Ryanodine Receptor Channels and Can Be Enhanced by Optogenetic Stimulation.

727   *Journal of Neuroscience* **34**: 15947-15956.

728 Sung KJ, Yang WL, Wu CB. 2019. Uncoupling neurotrophic function from nociception of nerve

729   growth factor: what can be learned from a rare human disease? *Neural Regen Res* **14**:

730   570-573.

731 Wang W, Wildes CP, Pattarabanjird T, Sanchez MI, Glober GF, Matthews GA, Tye KM, Ting

732   AY. 2017. A light- and calcium-gated transcription factor for imaging and manipulating

733   activated neurons. *Nat Biotechnol* **35**: 864-871.

734 Watson FL, Heerssen HM, Bhattacharyya A, Klesse L, Lin MZ, Segal RA. 2001. Neurotrophins

735   use the Erk5 pathway to mediate a retrograde survival response. *Nat Neurosci* **4**: 981-988.

736 Williams DW, Kondo S, Krzyzanowska A, Hiromi Y, Truman JW. 2006. Local caspase activity

737   directs engulfment of dendrites during pruning. *Nature neuroscience* **9**: 1234-1236.

738 Williams DW, Truman JW. 2005. Cellular mechanisms of dendrite pruning in Drosophila:

739   insights from in vivo time-lapse of remodeling dendritic arborizing sensory neurons.

740   *Development* **132**: 3631-3642.

741 Wu X, Zhang Y, Takle K, Bilsel O, Li Z, Lee H, Zhang Z, Li D, Fan W, Duan C et al. 2016.

742   Dye-Sensitized Core/Active Shell Upconversion Nanoparticles for Optogenetics and

743   Bioimaging Applications. *ACS Nano* **10**: 1060-1066.

744 Wu YI, Frey D, Lungu OI, Jaehrig A, Schlichting I, Kuhlman B, Hahn KM. 2009. A genetically

745   encoded photoactivatable Rac controls the motility of living cells. *Nature* **461**: 104-108.

746 Xiang Y, Yuan Q, Vogt N, Looger LL, Jan LY, Jan YN. 2010. Light-avoidance-mediating

747   photoreceptors tile the Drosophila larval body wall. *Nature* **468**: 921-926.

748   Xiao JH, Wong AW, Willingham MM, van den Buuse M, Kilpatrick TJ, Murray SS. 2010.

749   Brain-Derived Neurotrophic Factor Promotes Central Nervous System Myelination via a

750   Direct Effect upon Oligodendrocytes. *Neurosignals* **18**: 186-202.

751   Xiao Y, Tian W, Lopez-Schier H. 2015. Optogenetic stimulation of neuronal repair. *Curr Biol* **25**:

752   R1068-1069.

753   Yiu G, He Z. 2006. Glial inhibition of CNS axon regeneration. *Nat Rev Neurosci* **7**: 617-627.

754   Zhang K, Cui B. 2015. Optogenetic control of intracellular signaling pathways. *Trends*

755   *Biotechnol* **33**: 92-100.

756   Zhang K, Duan L, Ong Q, Lin Z, Varman PM, Sung K, Cui B. 2014. Light-mediated kinetic

757   control reveals the temporal effect of the Raf/MEK/ERK pathway in PC12 cell neurite

758   outgrowth. *PLoS One* **9**: e92917.

759   Zhao EM, Suek N, Wilson MZ, Dine E, Pannucci NL, Gitai Z, Avalos JL, Toettcher JE. 2019.

760   Light-based control of metabolic flux through assembly of synthetic organelles. *Nat*

761   *Chem Biol* **15**: 589-597.

762   Zhao EM, Zhang Y, Mehl J, Park H, Lalwani MA, Toettcher JE, Avalos JL. 2018. Optogenetic

763   regulation of engineered cellular metabolism for microbial chemical production. *Nature*

764   **555**: 683-687.

765   Zhou XX, Fan LZ, Li P, Shen K, Lin MZ. 2017. Optical control of cell signaling by single-chain

766   photoswitchable kinases. *Science* **355**: 836-842.

767

768

769   **Figures**

770
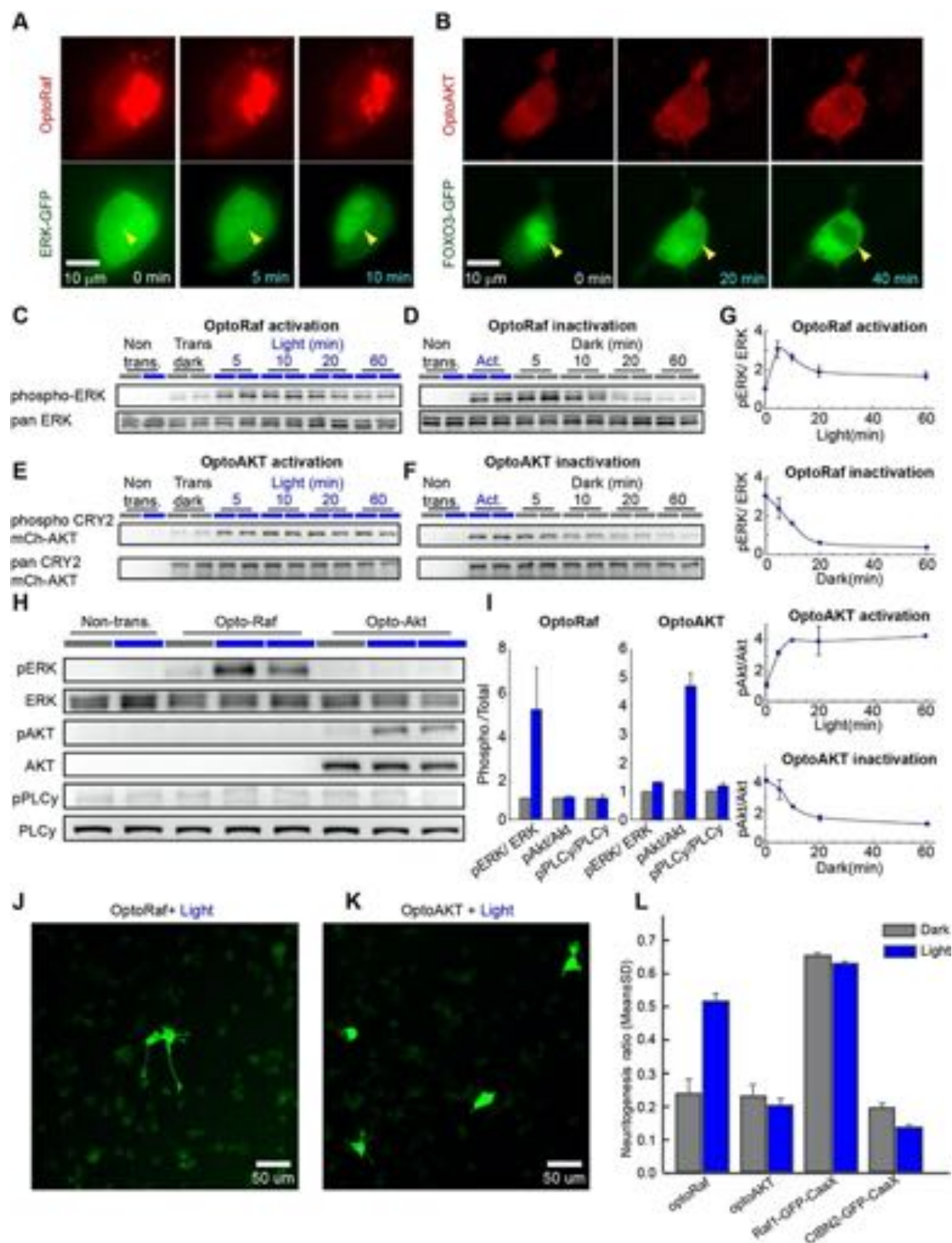
771 **Figure 1. OptoRaf and optoAKT specifically activate the ERK and AKT subcircuits,**

772 **respectively.** (*A*) Activation of optoRaf benchmarked with ERK-GFP nuclear translocation. (*B*)

773 Activation of optoAKT benchmarked with FOXO3-EGFP nuclear export. Scale bars = 10 μm. (*C*)

774 Western blot analysis of the pERK and ERK activities in response to time-stamped activation of

775 optoRaf. Blue light (0.5 mW/cm^2) was applied for 5, 10, 20, and 60 min to HEK293T cells

776 transfected with optoRaf. Non-transfected cells or optoRaf-transfected cells (dark) were used as

777 negative controls. (*D*) Inactivation of the pERK activity after blue light was shut off. (*E*) Western

778 blot analysis of the pAKT and AKT activities in response to time-stamped activation of

779 optoAKT. Cells were treated with identical illumination scheme in (C). (*F*) Inactivation of the

780 pAKT activity after blue light was shut off. (*G*) Quantification of the pERK activity (top two

781 panels) and pAKT (bottom two panels) upon optoRaf and optoAKT activation, respectively.

782 Both optoRaf and optoAKT show rapid (less than 5 min) and reversible activation patterns (*N* =

783 2). (*H*) OptoRaf and optoAKT do not show cross activity at the level of ERK and AKT. Neither

784 optoRaf nor optoAKT can cause PLCγ phosphorylation. Cells were exposed to blue light (0.5

785 mW/cm^2) for 10 min before lysis. (*I*) Quantification of the phosphorylated protein level in (H) (*N*

786 = 2). (*J*, *K*) PC12 cells transfected with either optoRaf (J) or optoAKT (K) were treated by blue

787 light for 24 h (0.2 mW/cm^2). Scale bars = 50 μm. (*I*) Quantification of the neuritogenesis ratio of

788 PC12 cells transfected with optoRaf or optoAKT. A membrane-targeted Raf (Raf1-GFP-CaaX)

789 causes constitutive neuritogenesis independent of light treatment, whereas the no-Raf (CIBN2-

790 GFP-CaaX) control does not increase the neuritogenesis ratio under light or dark treatment.

791

792

36

793

37
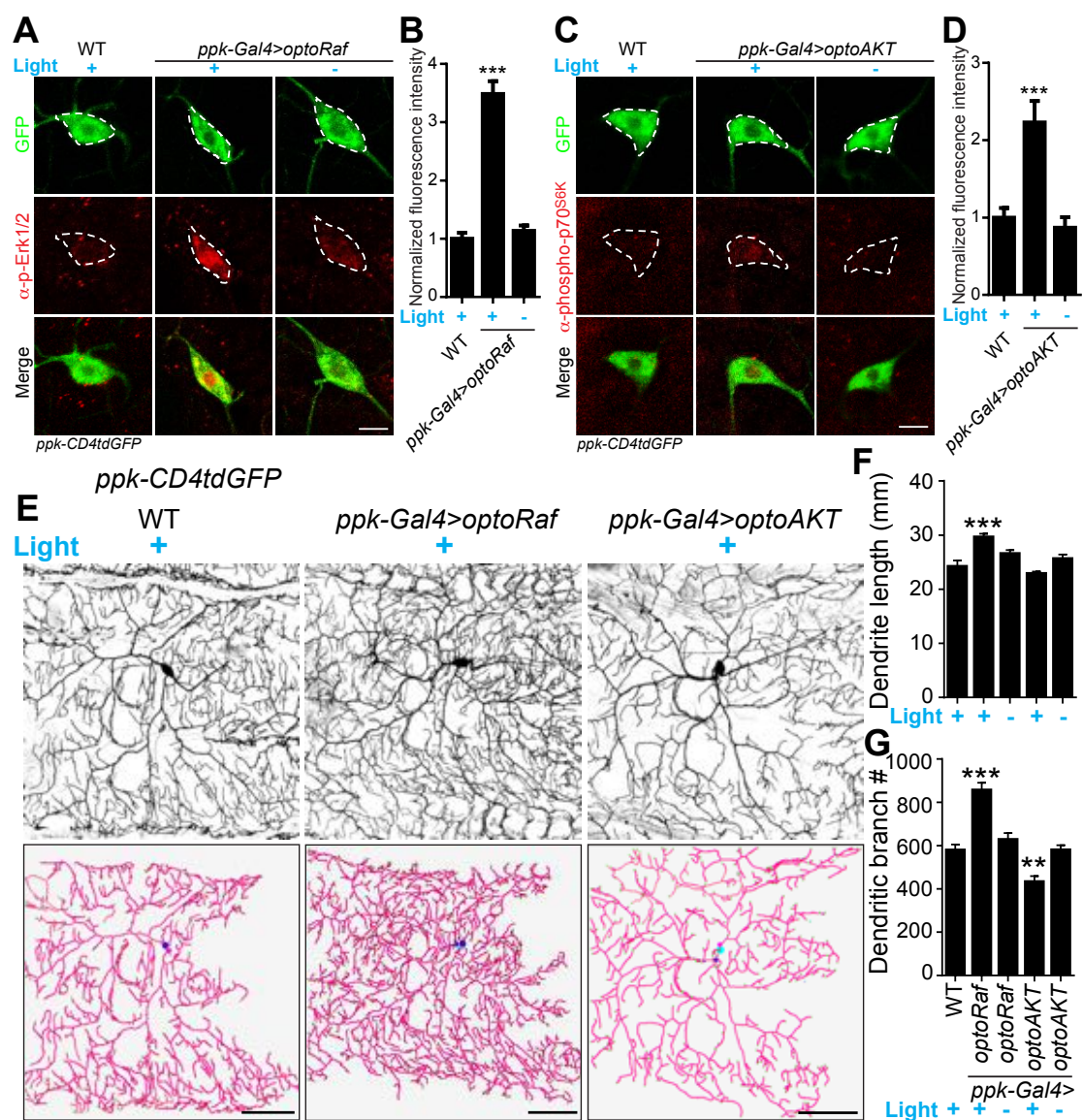
794 **Figure 2. Activation of optoRaf but not optoAKT increases C4da neuron dendrite**

795 **complexity.** (*A*, *B*) Blue light stimulation activates optoRaf in flies *in vivo*. (A) The body walls

796 from WT and optoRaf expressing larvae were dissected and stained for pERK1/2. After 5-min

797 continuous light stimulation, the relative intensity of pERK is significantly increased in the

798 optoRaf-expressing C4da neurons (labeled by *ppk-CD4tdGFP*). C4da neuron cell bodies are

799 outlined by dashed white lines. Scale Bar = 10 μm. (B) Qualification of pERK fluorescence

800 intensity in (A). The intensity of pERK in optoRaf expressing larvae was normalized to that of

801 WT. $N = 18$ neurons. (*C*, *D*) The 5-min light stimulation is sufficient to activate optoAKT *in vivo*.

802 (C) The larval body walls from WT and optoAKT expressing larvae were dissected and stained

803 for phospho-p70^{S6K}, a downstream component of the AKT pathway. Light stimulation increases

804 phospho-p70^{S6K} signal intensity in C4da neurons expressing optoAKT. C4da neuron cell bodies

805 are outlined by dashed white lines. Scale Bar = 10 μm. (D) Qualification of phospho-p70^{S6K}

806 fluorescence intensity in (C). The intensity of phospho-p70^{S6K} in optoAKT expressing larvae was

807 normalized to that of WT. WT (light) $N = 17$, *optoAKT* (light) $N = 19$, *optoAKT* (dark) $N = 18$

808 neurons. (*E-G*) Activation of Raf/MEK/ERK but not AKT signaling by 72 hours' light

809 stimulation increases dendrite outgrowth and branching in C4da neurons. (E) Representative

810 images of C4da neurons from WT, optoRaf and optoAKT expressing larvae with 72 hours' light

811 stimulation and the unstimulated controls. Neurons were reconstructed with Neurostudio. Scale

812 bar = 50 μm. (F) Quantification of total dendrite length of C4da neurons. (G) Qualification of

813 dendritic branch number. WT (light) $N = 21$, *optoRaf* (light) $N = 20$, *optoRaf* (dark) $N = 21$,

814 *optoAKT* (light) $N = 21$, *optoAKT* (dark) $N = 20$ neurons. All data are mean ± SEM. The data

815 were analyzed by one-way ANOVA followed by Dunnett's multiple comparisons test, **$P <$

816 0.01, ***$P < 0.001$.

38

817

818
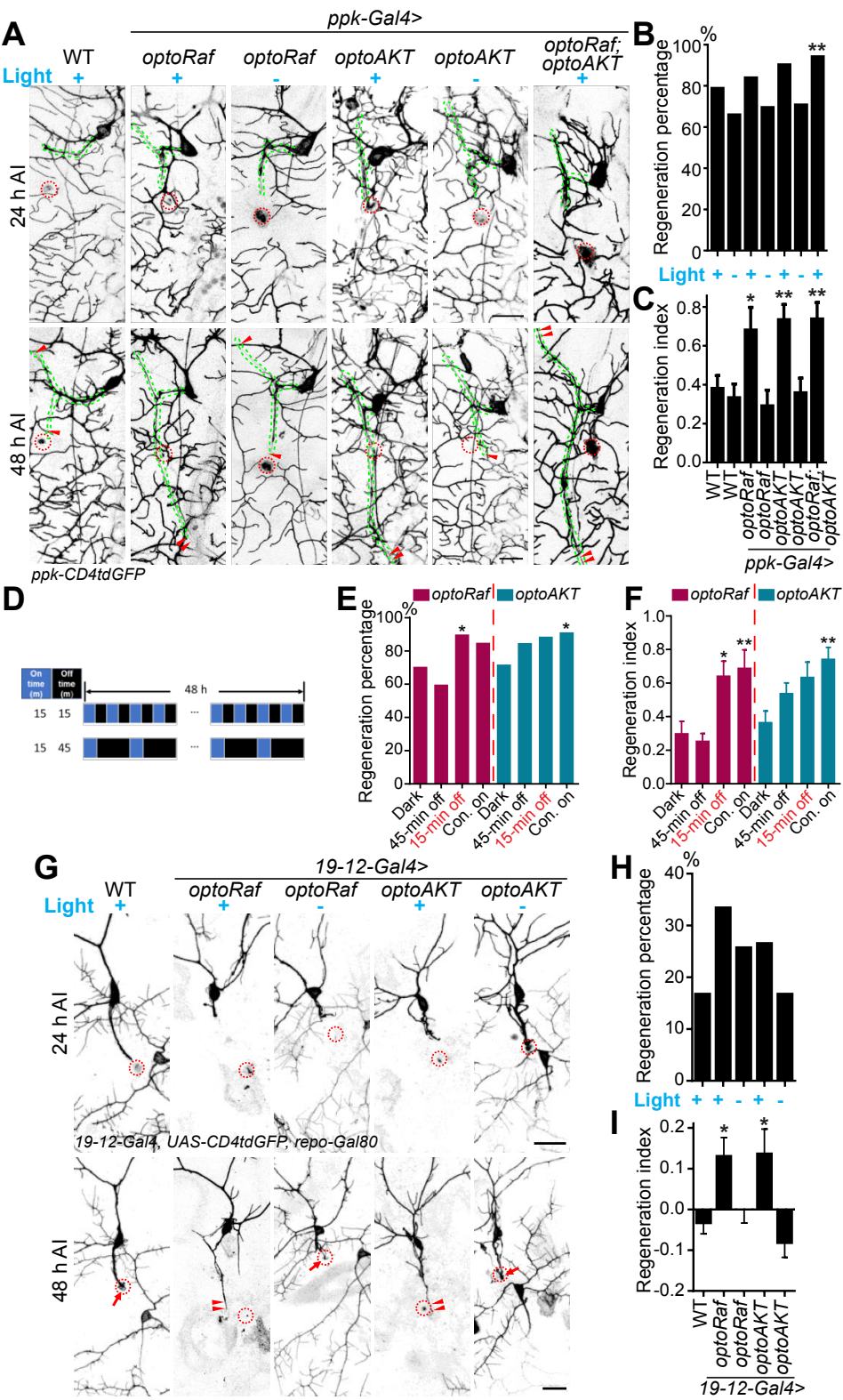
819   **Figure 3 Light-stimulated optoRaf or optoAKT enhances axon regeneration in the PNS.**

820   (*A-C*) Compared to WT, C4da neurons expressing optoRaf or optoAKT show significantly

821   increased axon regeneration in response to blue light. No enhancement was observed in the

822   unstimulated controls. (A) C4da neuron axons were severed and their regeneration was assayed

823   at 48 h AI. The injury site is marked by the dashed circle and regenerating axons are marked by

824   arrowheads. Axons are outlined with dashed green lines. Scale bar = 20 μm. (B) The

825   regeneration percentage of light-stimulated transgenic groups is not significantly higher than WT.

826   Fisher's exact test, $P = 0.2199$, $P = 0.6026$, $P = 0.8829$, $P = 0.1445$, $P = 0.7886$, $P = 0.0025$. (C)

827   Qualification of C4da neuron axon regeneration by the regeneration index. WT (light) $N = 33$,

828   WT (dark) $N = 41$, *optoRaf* (light) $N = 31$, *optoRaf* (dark) $N = 36$, *optoAKT* (light) $N = 52$,

829   *optoAKT* (dark) $N = 41$, *optoRaf + optoAKT* (light) $N=51$ neurons. Data are mean ± SEM,

830   analyzed by one-way ANOVA followed by Dunnett's multiple comparisons test. (*D-F*) After

831   injury, larvae were subjected to programmed light and dark cycles for a total of 48 h. The

832   intermittent light stimulation promotes axon regrowth in optoRaf expressing larvae similar to

833   constant light when the off-time is 15 min. (D) The intermittent patterns of the light stimulus. (E)

834   Compared to larvae incubated in dark, light stimulation is capable of increasing the percentage of

835   regenerated axons. Fisher's exact test, $P = 0.3357$, $P = 0.0422$, $P = 0.1673$; $P = 0.1414$, $P =$

836   0.0639, $P = 0.0307$. (F) Qualification of C4da axon regeneration by the regeneration index.

837   *OptoRaf* (dark) $N = 36$, *optoRaf* (45-min off) $N = 43$, *optoRaf* (15-min off) $N = 36$, *optoRaf* (Con.

838   on) $N = 31$, *optoAKT* (dark) $N = 41$, *optoAKT* (45-min off) $N = 49$, *optoAKT* (15-min off) $N = 40$,

839   *optoAKT* (Con. on) $N = 52$ neurons. Data are mean ± SEM, analyzed by one-way ANOVA

840   followed by Dunnett's multiple comparisons test. (*G-I*) Blue light stimulation significantly

841   enhances axon regeneration in the regeneration-incompetent C3da neurons. (G) C3da neuron

842   axon degeneration was verified at 24 h AI and axon regeneration was assessed at 48 h AI. The

843   injury site is marked by the dashed circle, regenerated axons are demarcated by arrowheads, and

844   arrow marks non-regenerated axons. Scale bar = 20 μm. (H) The regeneration percentage is not

845   significantly different. Fisher's exact test, $P = 0.0874$, $P = 0.9910$, $P = 0.2972$, $P = 1.0000$. (I)

846   Qualification of axon regeneration by the regeneration index. WT (light) $N = 41$, *optoRaf* (light)

847    $N = 36$, *optoRaf* (dark) $N = 39$, *optoAKT* (light) $N = 34$, *optoAKT* (dark) $N = 38$ neurons. Data are

848   mean ± SEM, analyzed by one-way ANOVA followed by Dunnett's multiple comparisons test.

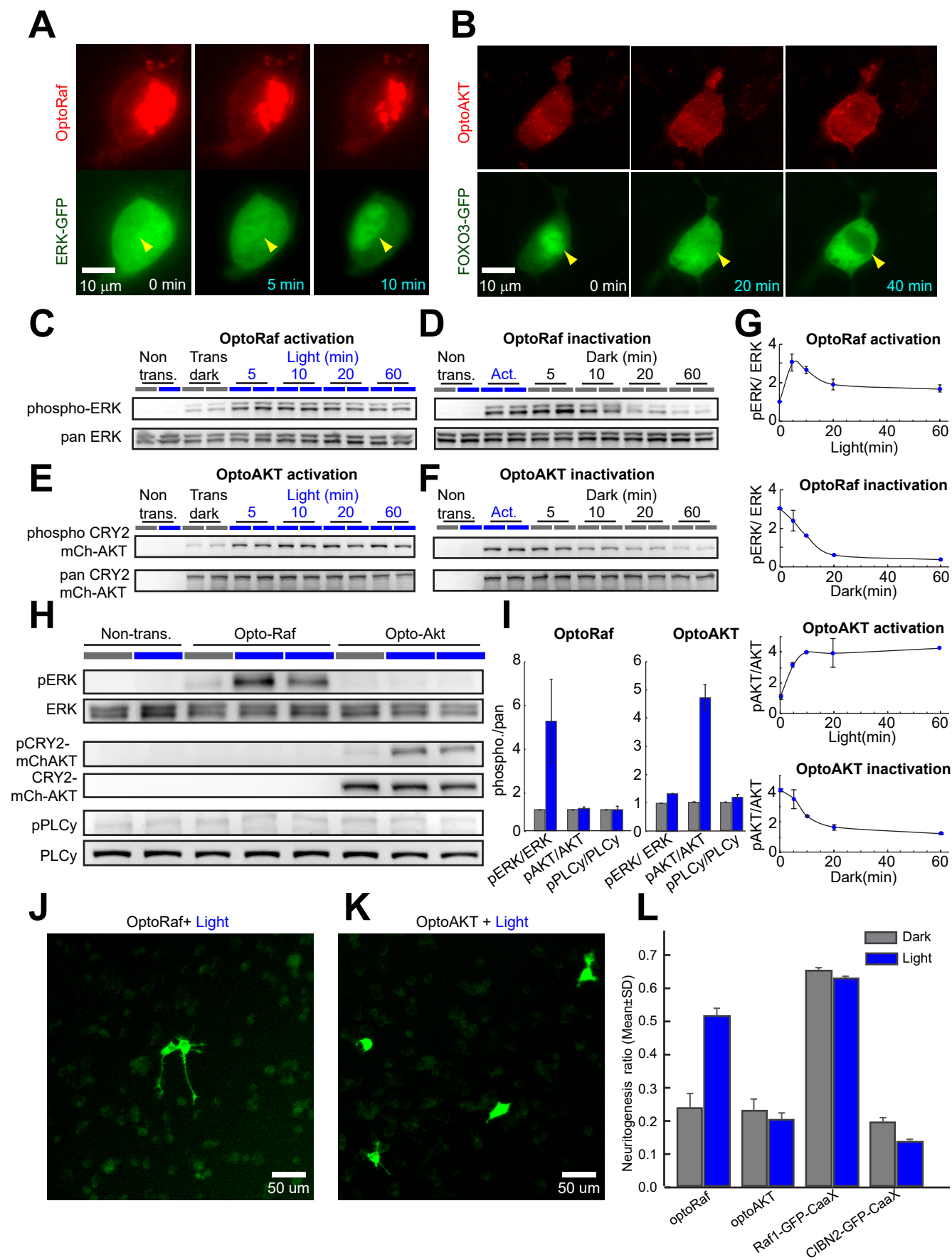849   *$P < 0.05$, **$P < 0.01$. See also Supplementary Fig. 2.

41

850

42
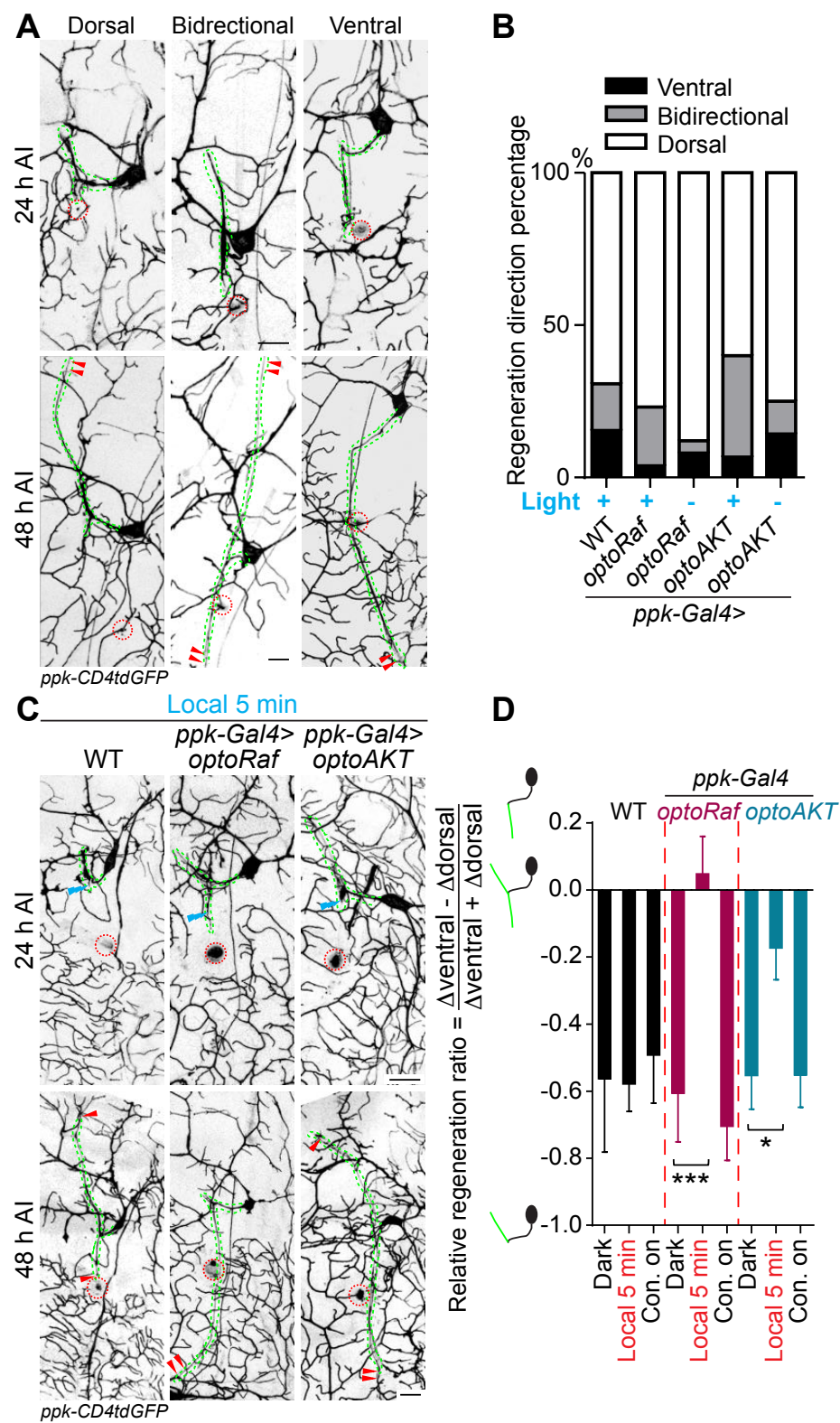
851 **Figure 4. Local optogenetic stimulation conveys guidance instructions to regenerating**

852 **axons.** (*A, B*) Regenerating axons prefer to regrow away from the original trajectory, with only a

853 minority of axons finding the correct path. (A) Representative images of axons retracting or

854 bifurcating at 24 h AI. At 48 h AI in WT, regenerating axons extend dorsally, ventrally, or both

855 directions. The injury site is marked by the dashed circles and regenerating axons are marked by

856 arrowheads. Axons are outlined with dashed green lines. Scale bar = 20 μm. (B) Light

857 stimulation fails to increase the percentage of axons regrowing towards the right direction. The

858 percentage of axons extending towards the correct trajectory (ventral + both) were analyzed by

859 Fisher's exact test, $P = 0.5318$, $P = 0.1033$, $P = 0.7778$, $P = 0.6363$. WT (light) $N = 26$, *optoRaf*

860 (light) $N = 26$, *optoRaf* (dark) $N = 25$, *optoAKT* (light) $N = 45$, *optoAKT* (dark) $N = 28$ neurons.

861 (*C, D*) Restricted local activation of optoRaf or optoAKT significantly increases the relative

862 regeneration ratio. The ratio is defined to weigh the regeneration potential of the ventral branch

863 against the dorsal branch. (C) A single pulse of light stimulation delivered specifically on the

864 ventral axon branch at 24 h AI (blue flash symbol) is capable of promoting preferential extension

865 of regenerating axons in optoRaf or optoAKT expressing larvae. (D) Qualification of the relative

866 regeneration ratio of v'ada. WT (dark) $N= 32$, WT (local 5 min) $N = 32$, WT (Con. on) $N = 33$,

867 *optoRaf* (dark) $N = 33$, *optoRaf* (local 5 min) $N = 35$, *optoRaf* (Con. on) $N = 35$, *optoAKT* (dark)

868 $N = 33$, *optoAKT* (local 5 min) $N = 34$, *optoAKT* (Con. on) N = 36 neurons. Data are mean ±

869 SEM, analyzed by one-way ANOVA followed by Dunnett's multiple comparisons test, *$P <$
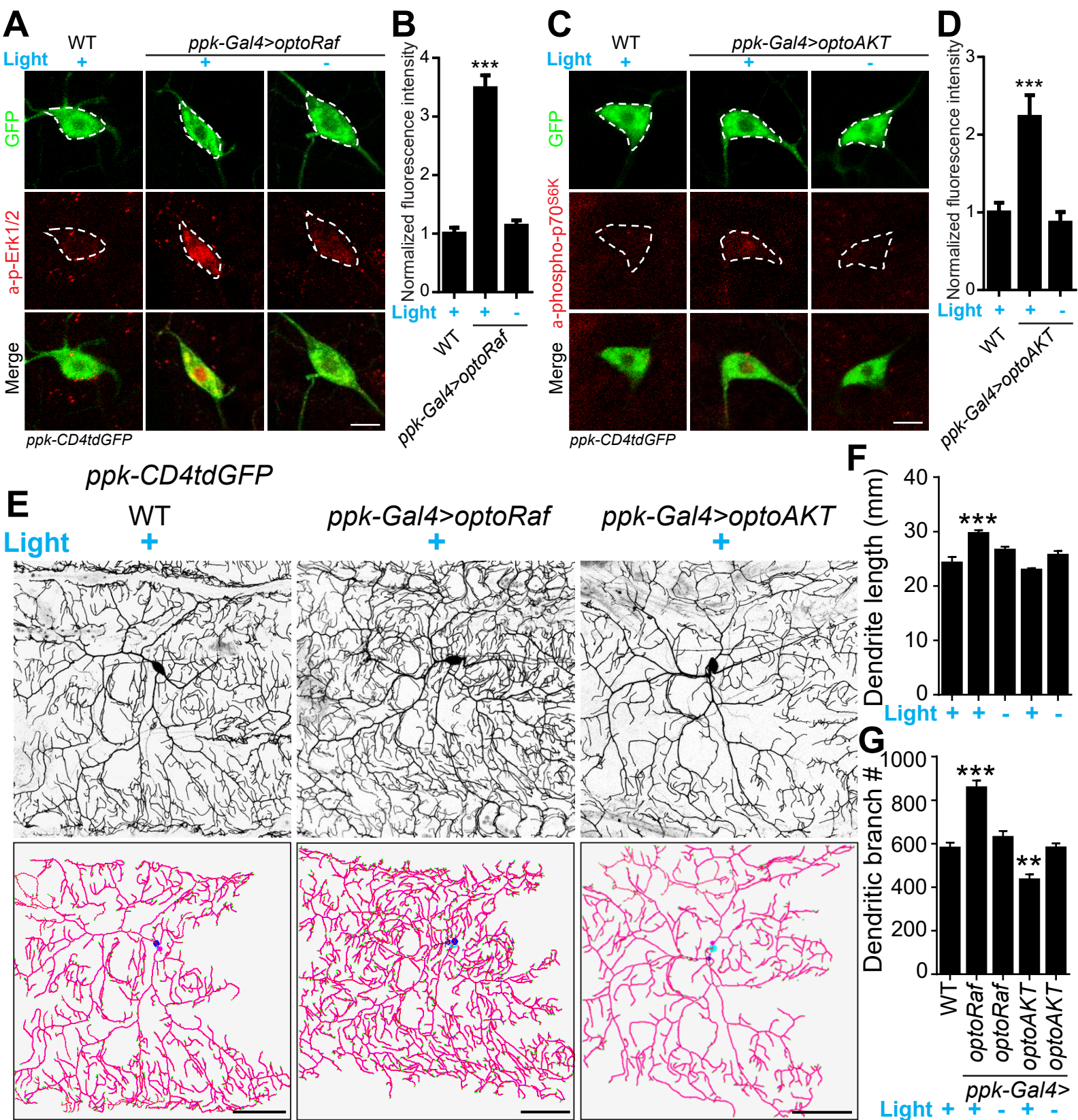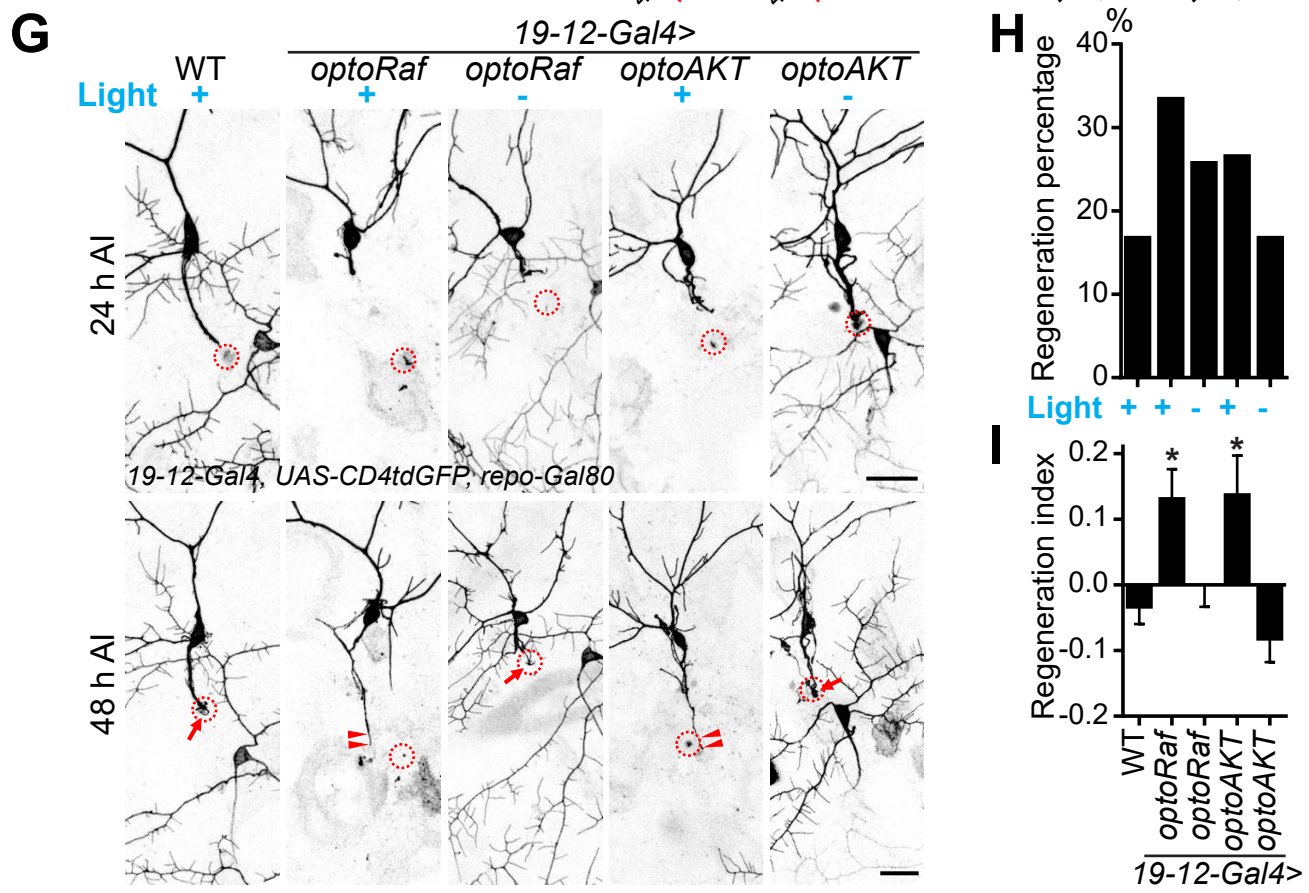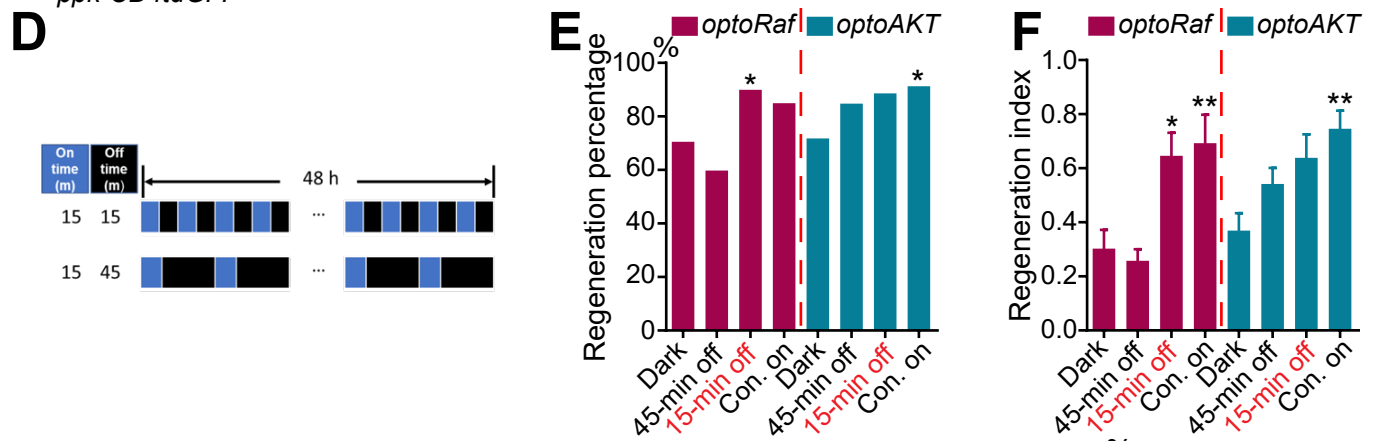
870 0.05, ***$P < 0.001$.

871
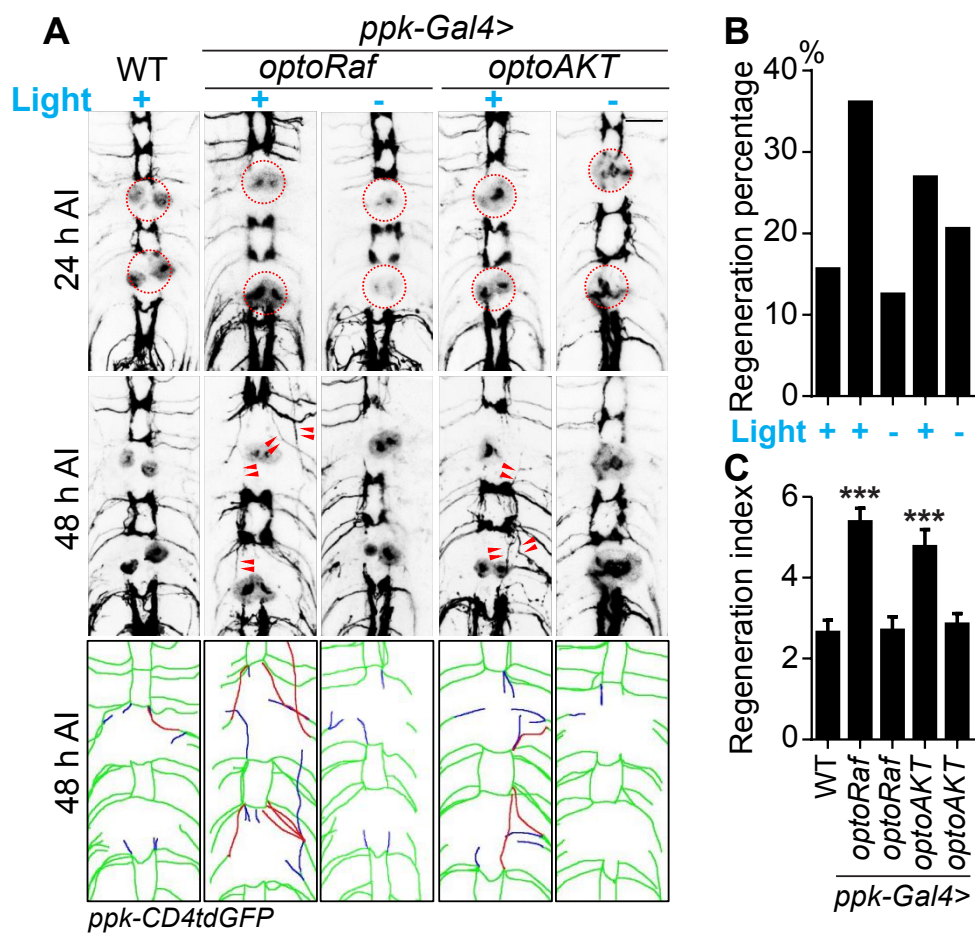
872 **Figure 5. Activation of optoRaf or optoAKT promotes axon regeneration in the CNS.** (*A-C*)

873 Light stimulation significantly enhances axon regeneration in the VNC of optoRaf or optoAKT

874 expressing larvae. (A) Complete degeneration in A3 and A6 commissure segments was

875 confirmed at 24 h AI and regeneration of these two segments was assayed independently at 48 h

876 AI. The injury site is marked by the dashed circle and regenerating axons are labeled by

877 arrowheads. In the schematic diagrams, regrowing axons that reached other bundles and thus

878 define a regenerating commissure segment are highlighted in red, while other regrowing axons

879 are illustrated in blue. Scale bar = 20 μm. (B) The regeneration percentage is not significantly

880 different. Fisher's exact test, $P = 0.0560$, $P = 0.7192$, $P = 0.2908$, $P = 0.6013$. (C) Qualification

881 of axon regeneration in VNC by the regeneration index. WT (light) $N = 32$, *optoRaf* (light) $N =$

882 36, *optoRaf* (dark) $N = 32$, *optoAKT* (light) $N = 26$, *optoAKT* (dark) $N = 34$ segments. Data are

883 mean ± SEM, analyzed by one-way ANOVA followed by Dunnett's multiple comparisons test,

884 ****P* < 0.001. See also Supplementary Fig. 3.

885

886

887
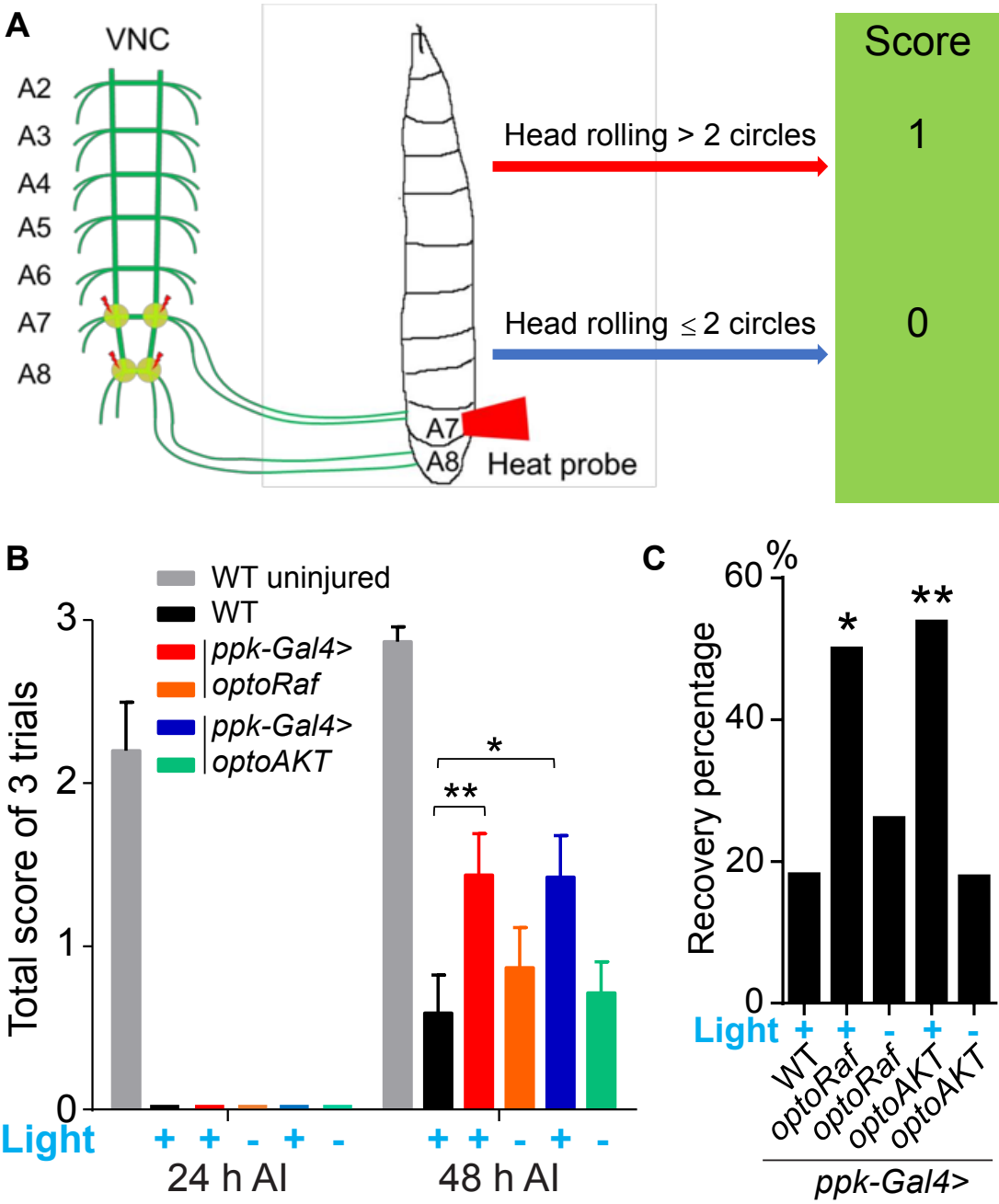
888 **Figure 6. Activation of optoRaf or optoAKT promotes functional regeneration after CNS**

889 **injury.** (*A*) A schematic drawing of the behavioral recovery test. The A7 and A8 C4da neuron

890 axon bundles (corresponding to the A7 and A8 body segments) in the VNC were injured by laser

891 and the larva was then subjected to three consecutive trials at 24 and 48 h AI, respectively. In

892 each trial, a 47°C heat probe was applied at the A7 or A8 segments. A fully recovered larva

893 would produce a stereotypical rolling behavior in response to the heat probe and would be scored

894 as "1", otherwise as "0". If the total score of the three trials was below 1 at 24 h AI but increased

895 to 2 or 3 at 48 h AI, the larva was defined as recovered. (*B*, *C*) Behavioral recovery test was

896 performed at 24 h and 48 h after VNC injury (A7 and A8 bundles). Larvae expressing optoRaf or

897 optoAKT exhibit significantly accelerated recovery in response to light stimulation. (B)

898 Qualification of the total scores at each time point. WT (uninjured) $N = 15$, WT (light) $N = 22$,

899 *optoRaf* (light) $N = 32$, *optoRaf* (dark) $N = 23$, *optoAKT* (light) $N = 26$, *optoAKT* (dark) $N = 28$.

900 Data are mean ± SEM, analyzed by two-way ANOVA followed by Tukey's multiple

901 comparisons test. (C) Qualification of the recovery percentage. The data were analyzed by

902 Fisher's exact test, $P = 0.0174$, $P = 0.5237$, $P = 0.0052$, $P = 0.9763$. *$P < 0.05$, **$P < 0.01$.
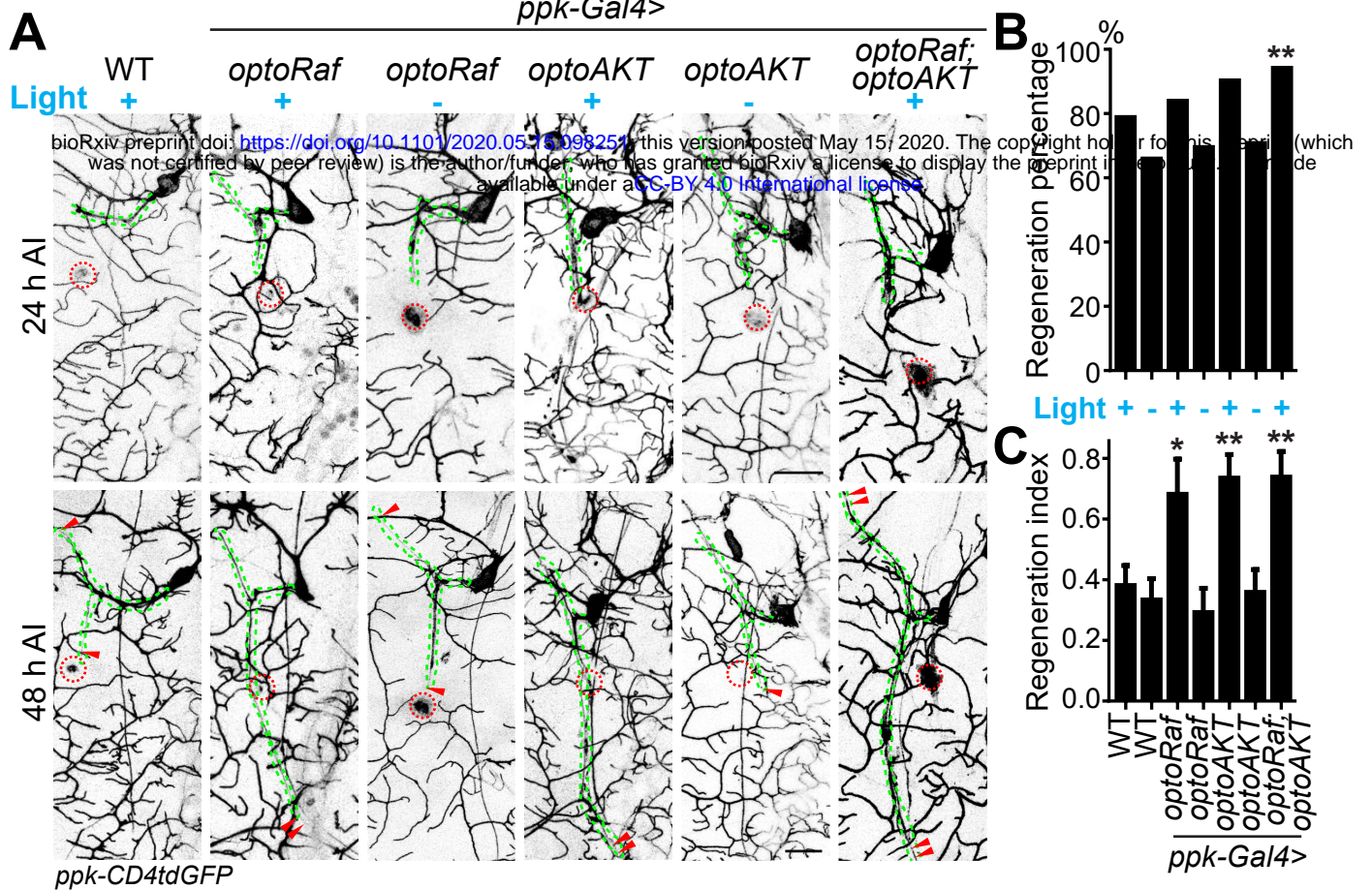
903

A

Dorsal Bidrectional Ventral

24 h AI

48 h AI

ppk-CD4tdGFP

B

Regeneration direction percentage %

Ventral
Bidirectional
Dorsal

100

50

0

Light + + - + -

WT *optoRaf* *optoRaf* *optoAKT* *optoAKT*

ppk-Gal4>

C

Local 5 min

WT *ppk-Gal4>* *ppk-Gal4>*
optoRaf *optoAKT*

24 h AI

48 h AI

ppk-CD4tdGFP

D

$$\text{Relative regeneration ratio} = \frac{D_{ventral} - D_{dorsal}}{D_{ventral} + D_{dorsal}}$$

ppk-Gal4

WT *optoRaf* *optoAKT*

0.2

0.0

-0.2

-0.4

-0.6

-0.8

-1.0

Dark Local 5 min Con. on Dark Local 5 min Con. on Dark Local 5 min Con. on

***

*

ppk-CD4tdGFP

A

VNC

A2
A3
A4
A5
A6
A7
A8

Head rolling > 2 circles → Score 1

Head rolling ≤ 2 circles → Score 0

A7
A8 Heat probe

B

WT uninjured
WT
ppk-Gal4>
optoRaf
ppk-Gal4>
optoAKT

Total score of 3 trials

Light: + + - + -   + + - + -

24 h AI   48 h AI

C

Recovery percentage (%)

Light: + + - + -

WT *optoRaf* *optoRaf* *optoAKT* *optoAKT*

ppk-Gal4>
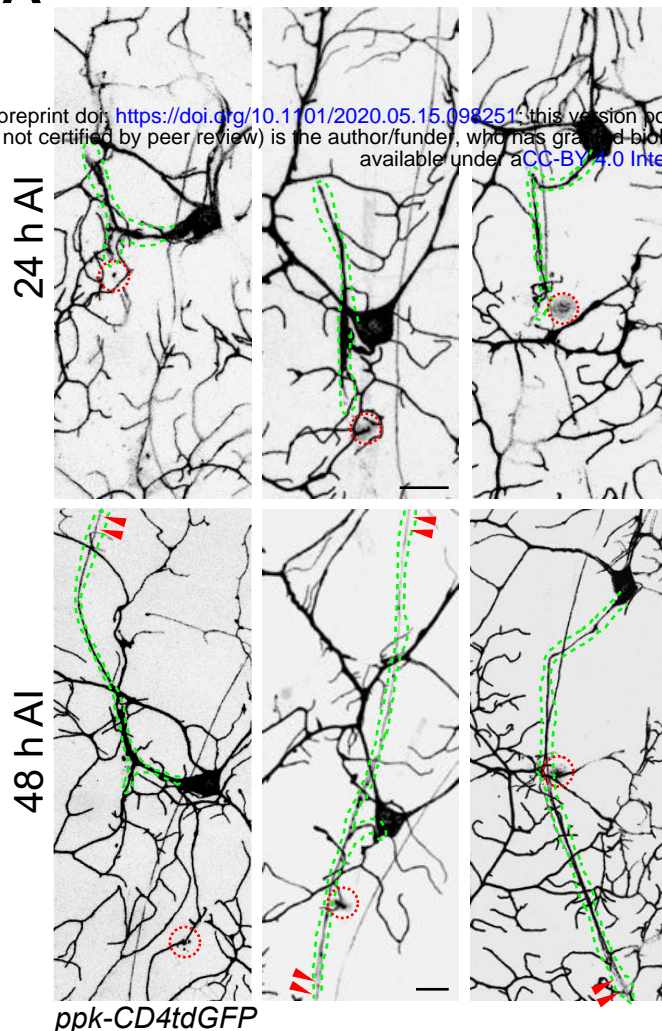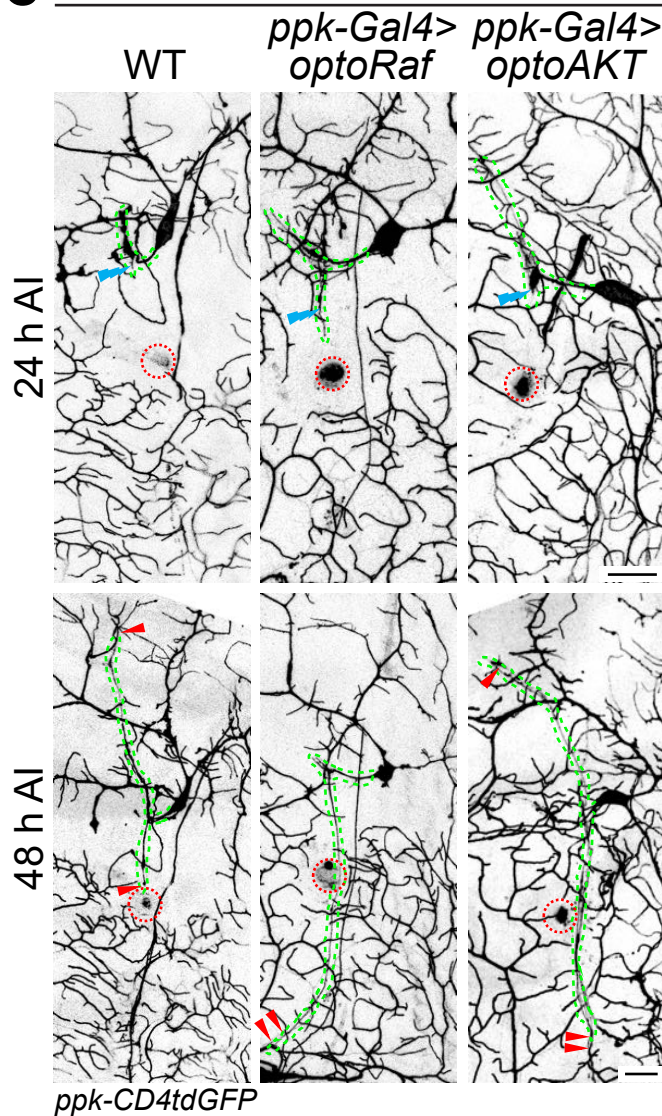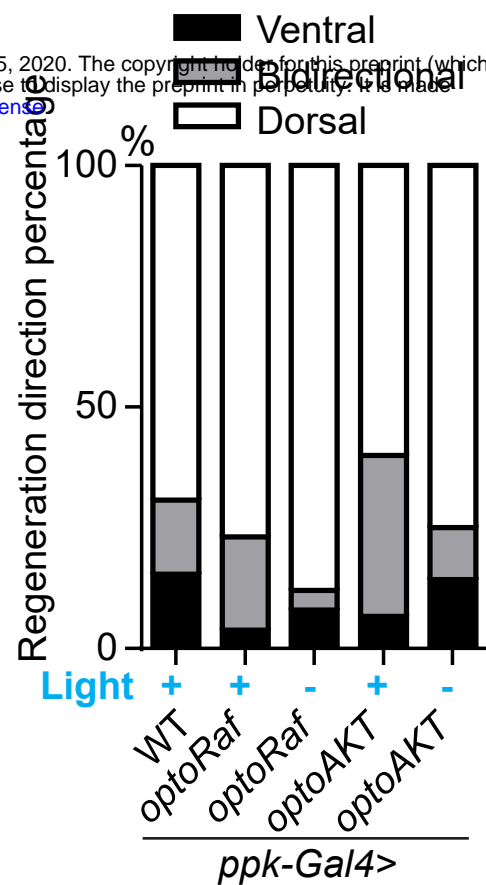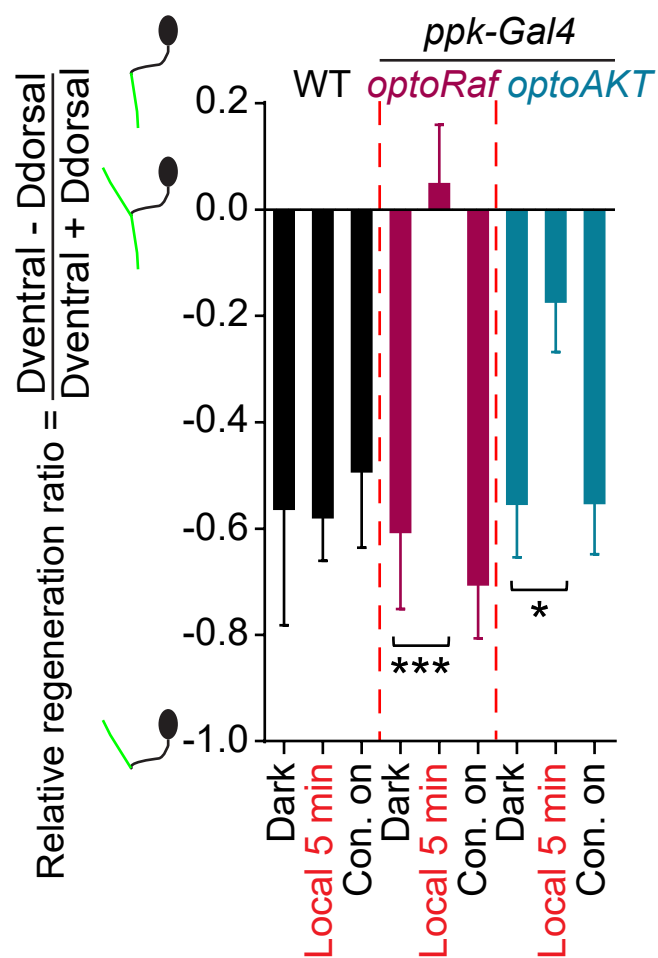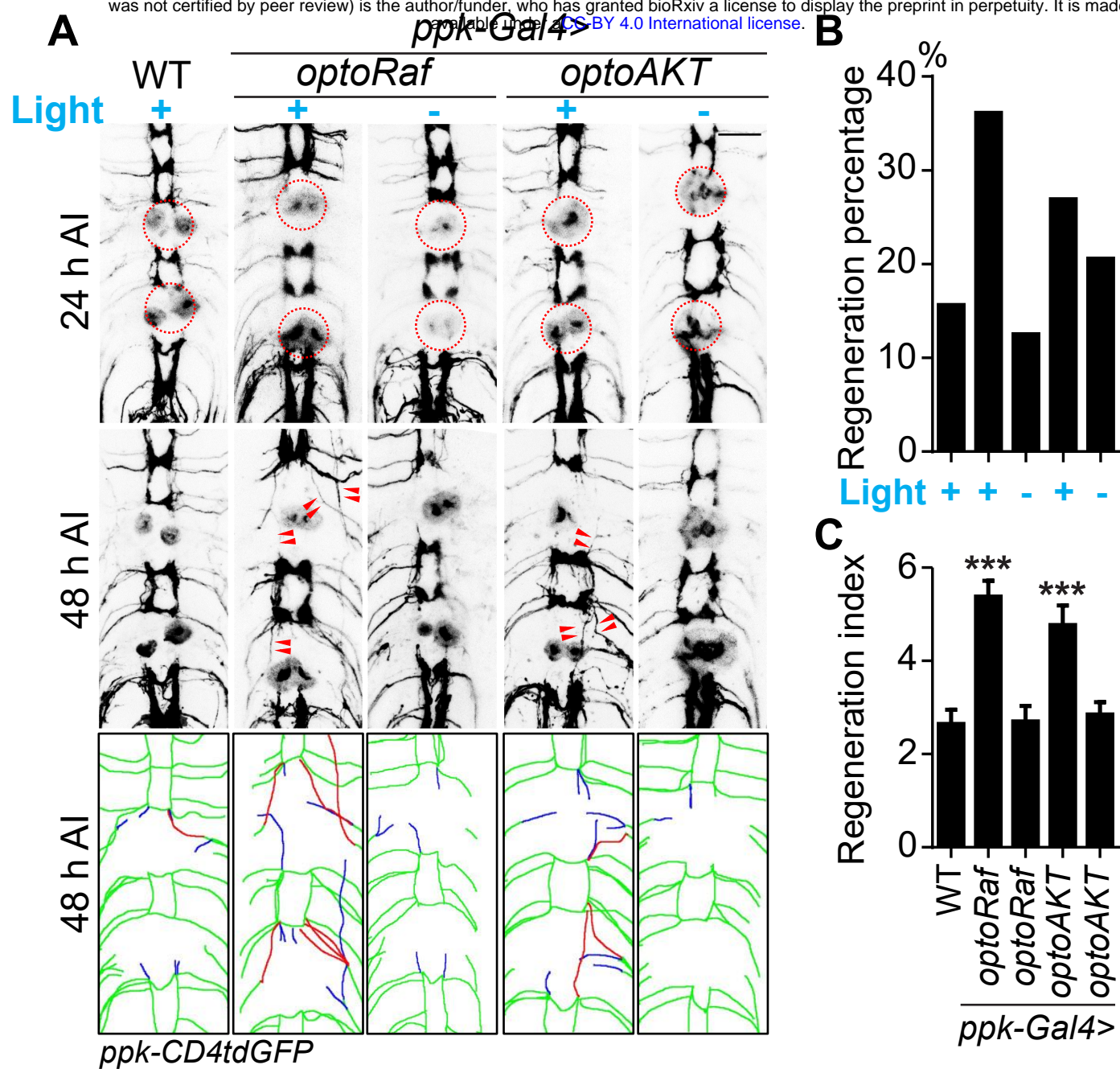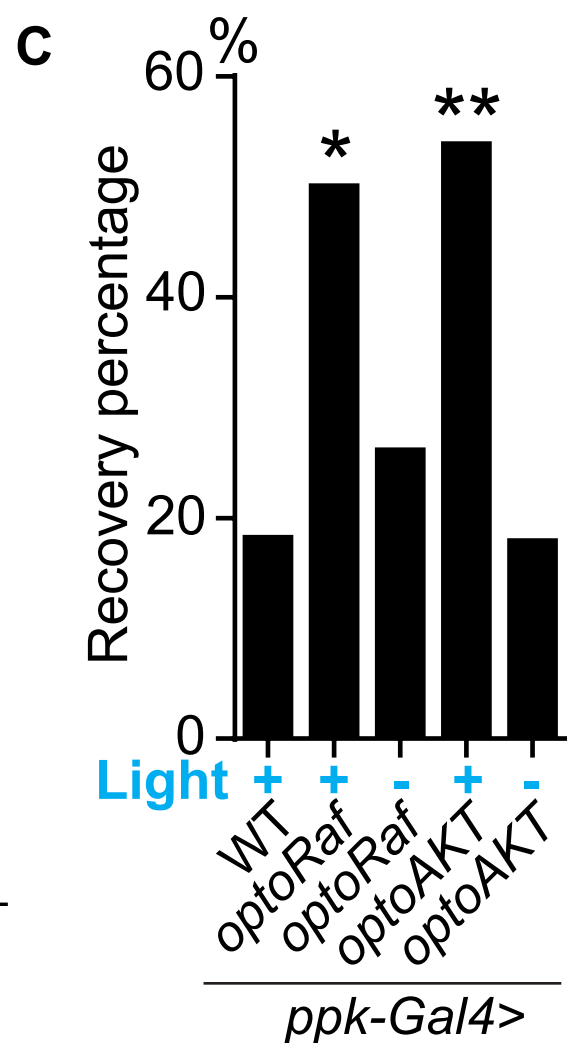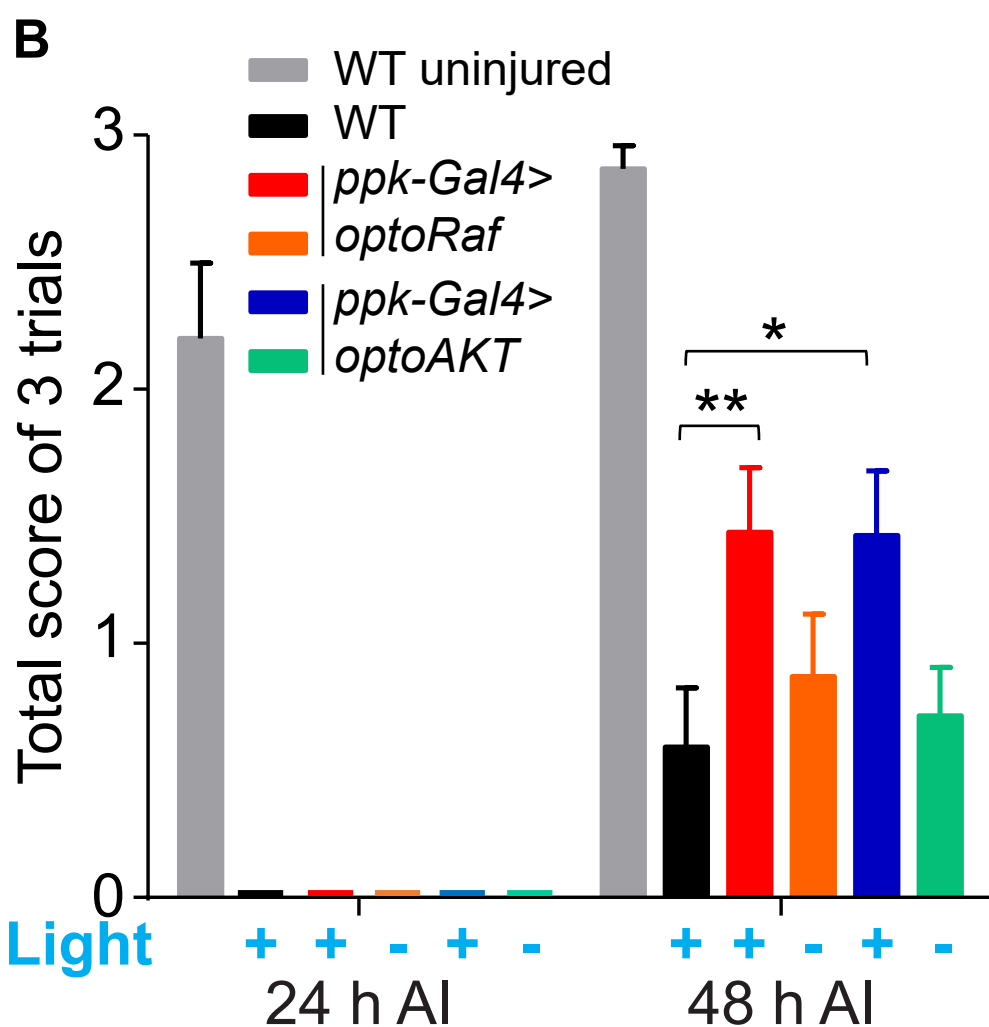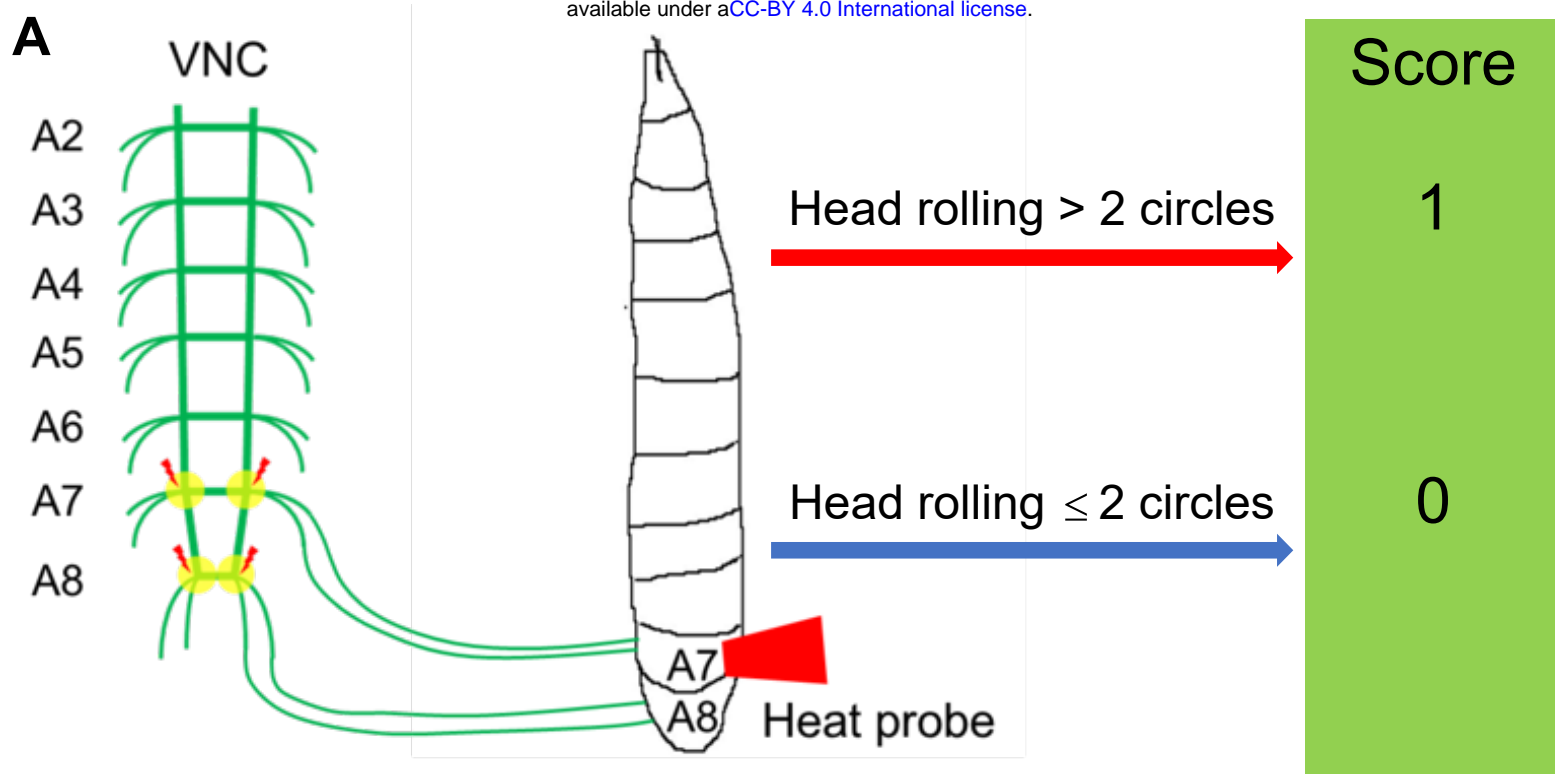
Supplemental Data

Optical control of ERK and AKT signaling promotes axon regeneration and functional recovery of PNS and CNS in *Drosophila*

Qin Wang[1,2], Huaxun Fan[3], Feng Li[1,2], Savanna S. Skeeters[3], Vishnu Krishnamurthy[3], Yuanquan Song[1,2,*], Kai Zhang[3,4,5,6,*]

[1]Raymond G. Perelman Center for Cellular and Molecular Therapeutics, The Children's Hospital of Philadelphia, Philadelphia, PA 19104, USA

[2]Department of Pathology and Laboratory Medicine, University of Pennsylvania, Philadelphia, PA 19104, USA

[3]Department of Biochemistry, [4]Neuroscience Program, [5]Center for Biophysics and Quantitative Biology, [6]Beckman Institute for Advanced Science and Technology, University of Illinois at Urbana-Champaign, Urbana, IL 61801, USA

*Correspondence and requests for materials should be addressed to Y.S. (email: songy2@email.chop.edu) or to K.Z. (email: kaizkaiz@illinois.edu).

Contents

Supplementary Figures of the quantification of axon regeneration in the PNS and axon regeneration in the CNS.

Supplementary movies of reversible optogenetic stimulation of Raf and AKT membrane recruitment, nuclear translocation of ERK, nuclear retreatment of FOXO3-GFP with optoRaf resolved by live-cell imaging:

Movie S1: Reversible optogenetic stimulation of Raf membrane recruitment with optoRaf resolved by live-cell imaging in BHK21 cells.

Movie S2: Reversible optogenetic stimulation of AKT membrane recruitment with optoAKT resolved by live-cell imaging in BHK21 cells.

Movie S3: Optogenetic activation of optoRaf causes nuclear translocation of ERK-GFP in BHK21 cells.

Movie S4: Optogenetic activation of optoAKT causes retreatment of FOXO3-GFP from the nucleus into the cytoplasm in BHK21 cells.
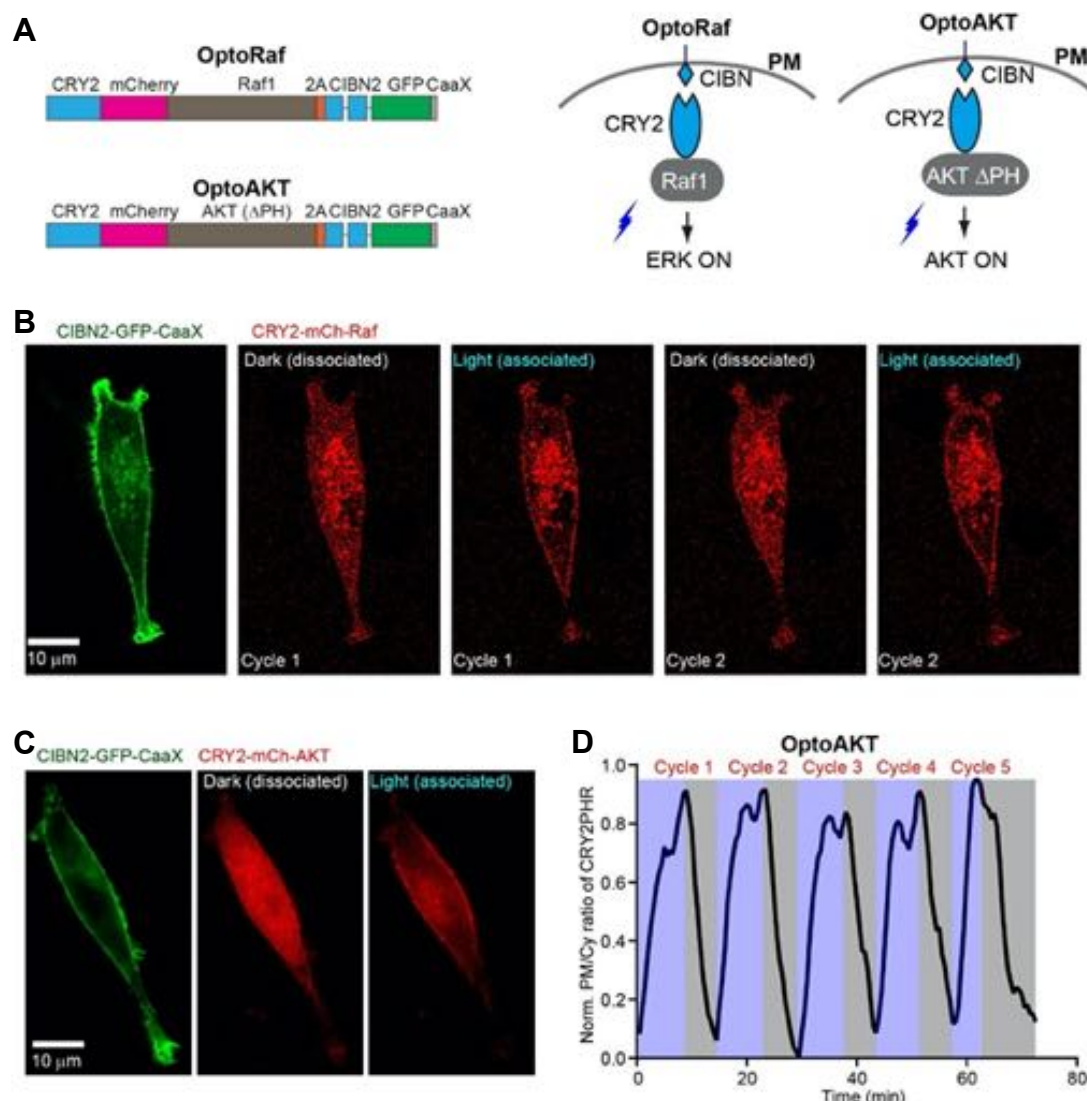
Supplementary Figure 1. Design and live cell imaging for optoRaf and optoAKT in mammalian cell cultures. (*A*) Blue light illumination facilitates the association of CIBN and CRY2, and the CIBN/CRY2 complex spontaneously dissociates in the dark. In both optoRaf and optoAKT, CIBN-GFP-CaaX anchors to the plasma membrane and the cytosolic signaling protein was fused to CRY2. Under blue light stimulation, optoRaf and optoAKT recruit the signaling protein, Raf1 (optoRaf) and AKT ΔPH (optoAKT) to the plasma membrane to activate the ERK and AKT signaling pathway, respectively. (*B, C*) Live-cell imaging of reversible membrane recruitment of CRY2-mCh-Raf (B) CRY2-mCh-AKT (C). After each cycle of light stimulation, cells were kept in the dark for about 30 min. (*D*) Multiple cycles of membrane recruitment can be achieved from the same cell.
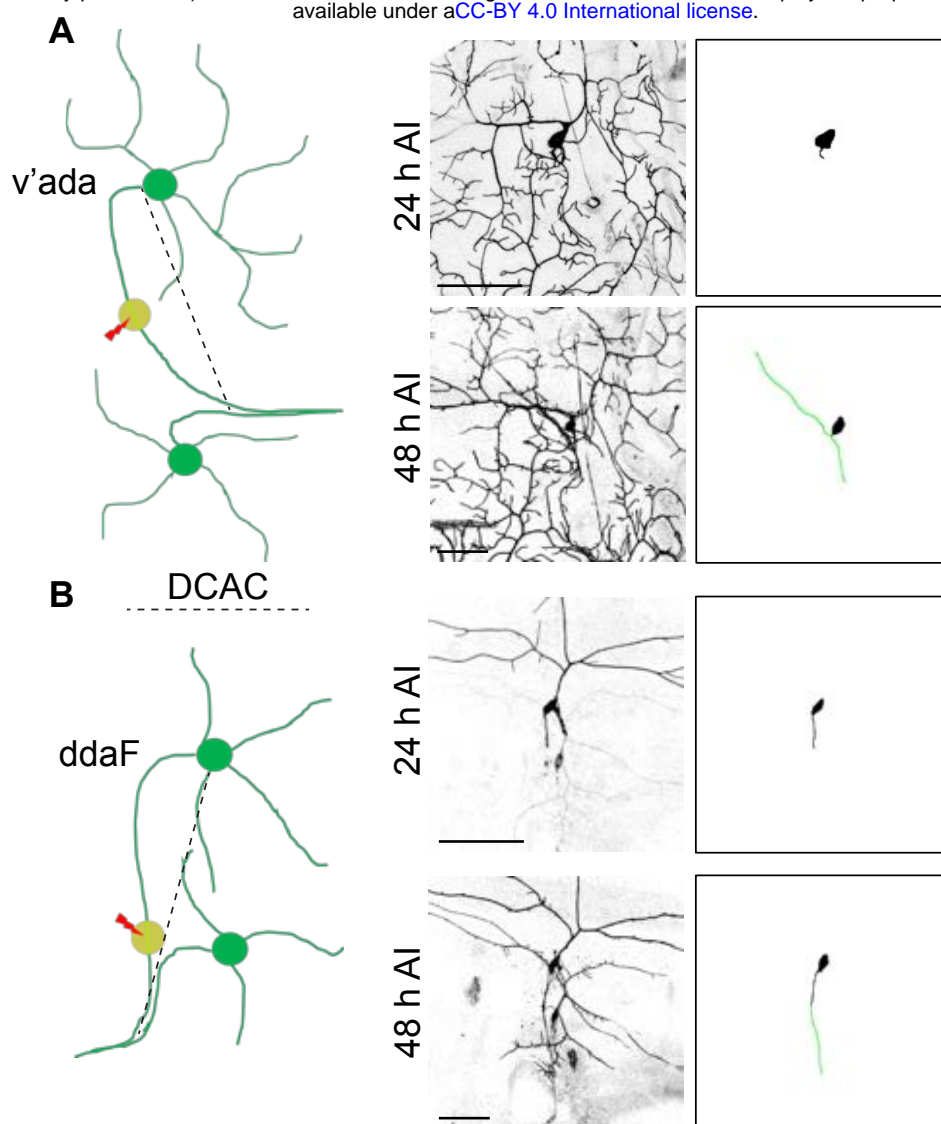
Supplementary Figure 2. Quantification of axon regeneration in the PNS. (*A*) A schematic diagram depicts the C4da neuron injury model. At 48 h AI, two branches of the regenerating axon are extended towards two opposite directions. To calculate the regeneration index, the increased length of the longer branch was measured and normalized by DCAC (the distance between the cell body and the axon converging point). Scale bar = 50 μm. (*B*) A schematic drawing depicts the C3da neuron injury model. The green line depicts the regenerated axon. Scale bar = 50 μm. Related to **Figure. 3**.
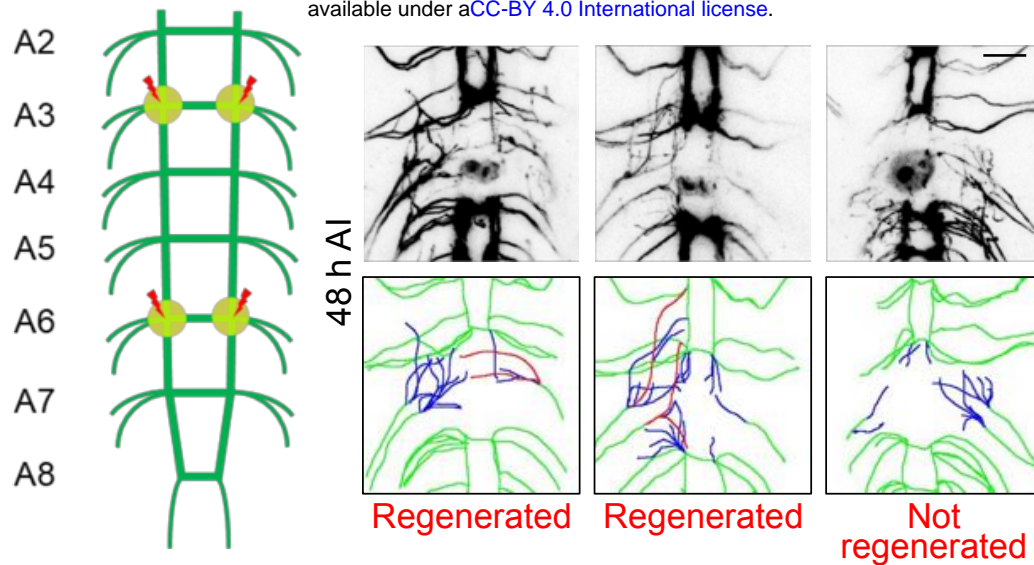
Supplementary Figure 3. Quantification of axon regeneration in the CNS. A schematic diagram of the VNC injury method. The abdominal A3 and A6 bundles were injured by laser and the regeneration of these two commissure segments were assessed independently at 48 h AI. The regeneration index is defined as the total length of all regenerated axons normalized to the length between A4 and A5 bundles. However, a commissure segment is defined as regenerated only when at least one axon extends beyond the midline of the commissure region or connects with other intact bundles. Those axons are illustrated in the schematic diagrams in red, while other regrowing axons are in blue. Scale bar = 20 μm. Related to **Figure. 5**.